SEMMELWEIS EGYETEM

DOKTORI ISKOLA

Ph.D. értekezések

3493.

JURÁNYI ESZTER PETRA

Celluláris és molekuláris élettan

című program

Programvezető: Dr. Hunyady László, egyetemi tanár

Témavezető: Dr. Nagy Péter, egyetemi tanár

Investigations of metabolic pathways of Reactive Sulfur Species

PhD thesis

Eszter Petra Jurányi

Semmelweis University Doctoral College

Molecular Medicine Division

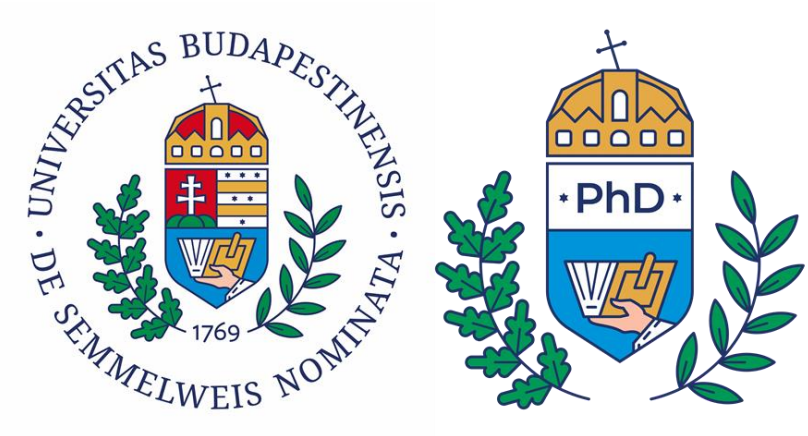

Supervisor: Péter Nagy PhD, DSc

Official reviewers: Jon M. Fukuto PhD

Tamás Kardon PhD

Head of the Complex Examination Committee:
Miklós Geiszt PhD, DSc

Members of the Complex Examination Committee:

Blanka Tóth PhD

Orsolya Mészáros-Kapuy PhD

Budapest
2026

Table of Contents

List of abbreviations

AOAA	aminooxoacetic acid
Cbs	Cystathionine-ß-synthase
Cse	Cystathionine-γ-lyase
CSH	cysteine
CSSC	cystine
CSSH	cysteine-persulfide
Cth	cystathionine
GSH	glutathione
GSSH	glutathione-persulfide
HMW	High Molecular Weight
HPE-IAM	(β-hydroxyphenyl)ethyl iodoacetamide
HPLC	High Performance Liquid Chromatography
LMW	Low Molecular Weight
MS/MS	tandem Mass Spectrometry
NADPH	Nicotinamide Adenine Dinucleotide Phosphate
PAG	propargyl-glycine
PDAC	pancreatic ductal adenocarcinoma
PLP	pyridoxal-5-phosphate
RSS	Reactive Sulfur Species
TR/GR-null	Thioredoxin Reductase and Glutathione disulfide Reductase-deficient mouse
WT	wild type

1 Introduction

Intracellular redox balance is essential for cellular viability, proliferation, and the regulation of processes ranging from energy metabolism and signal transduction to stress adaptation (1). Redox imbalance causes oxidative or reductive stress at the cellular level; moreover, several diseases are characterized by an impaired redox state (2), including cardiovascular (3, 4) and neurodegenerative diseases (5-7), metabolic disorders (8, 9), and cancer (10-13).

For a long time, oxidants and the production of Reactive Oxygen Species (ROS) were known as products of undesirable biological effects and damaging processes; however, that perception has changed. Today, we know that endogenously produced ROS play an important biological role, for example, in signaling. Reactive oxidants are continuously generated by intracellular and extracellular sources; therefore, a fine-tuned regulatory system is necessary to buffer redox fluctuations to prevent redox imbalance (1).

Similarly, hydrogen sulfide (H_2S) was known only as a highly toxic molecule but has now emerged as a small signaling molecule, or sometimes also called “gasotransmitter” (14), with a significant role in redox regulation (14, 15). Reactive Sulfur Species (RSS) have been recognized lately as critical regulators of redox homeostasis. Multivalent oxidation states, high polarizability, and labile S-S bonds are unique chemical properties of RSS (16), which grant them redox flexibility that exceeds that of classical antioxidant systems. RSS exhibits promiscuous reactivity, including nucleophilic, electrophilic (14), and radical-scavenging activities (17, 18). This chemical versatility and their high reactivity position them as central components of intracellular redox homeostasis, and make them capable of buffering oxidative stress while simultaneously modulating signaling pathways and other cellular events (1).

1.1 Reactive Sulfur Species

The term RSS refers to various sulfur-containing compounds that share the property of high reactivity, although their biologically relevant reactions can largely differ.

The most studied members of RSS are shown in Figure 1, along with a suggested grouping. RSS encompasse both organic and inorganic sulfur species. Inorganic RSS primarily consist hydrogen sulfide and its polysulfur derivatives, along with their

oxidized counterparts. In addition, due to crosstalk between the small signaling molecules, nitric oxide and H_2S, hybrid molecules such as SNO- and SSNO- can also be generated. These hybrid species can be classified as either reactive nitrogen species (RNS) or RSS (19).

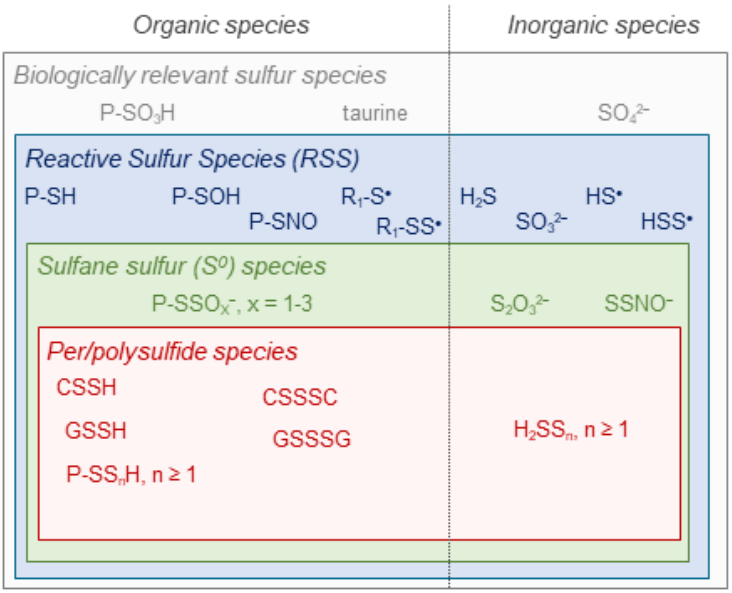

Figure 1. ***Classification of sulfur-containing compounds and Reactive Sulfur Species (RSS)****, adapted from Multifaceted Roles for Persulfide Species in Redox Chemical Biology (13). Abbreviations not mentioned in the text: P: protein, R_1: organic chain; CS: cysteine derivatives, GS: glutathione derivatives*

Within the realm of RSS, where two or more sulfur atoms are linked, a distinctive state of sulfur occurs, characterized by an oxidation state of 0, referred to as sulfane sulfur, which leads to greater reactivity and a broader range of reactions. Besides thiols and H_2S, the most biologically relevant species are the per- and polysulfides, which have a terminal SSH group. RSS also includes small-molecule (Low Molecular Weight (LMW)) persulfides and protein (High Molecular Weight (HMW)) persulfides (P-S_nSH, $n \geq 1$), which have distinct biological functions and are involved in different metabolic pathways.

1.2 Metabolic pathways of RSS

RSS can be produced enzymatically (plain arrows) and non-enzymatically (dashed arrows) as shown in Figure 2. The main source of RSS inside cells is cysteine (CSH). There are two known cellular sources of CSH; the most predominant is the reduction of cystine (CSSC) taken up by xCT (SLC7A11), the CSSC/glutamate antiporter (20, 21).

TRP14 then acts as the main enzyme to catalyze CSSC reduction to produce CSH. Under CSSC-deprived or TRP14-deficient conditions, CSH can also be produced through the transsulfuration pathway, where the sulfur is transferred from methionine (Met) to serine (Ser) (22). Cystathionine-ß-synthase (Cbs) and cystathionine-γ-lyase (Cse) are the two key enzymes in this pathway; their canonical functions are cystathionine formation from Ser and homocysteine (Hcys) (reaction 1) and the cleavage of cystathionine (Cth) to form CSH (reaction 2), respectively (23).

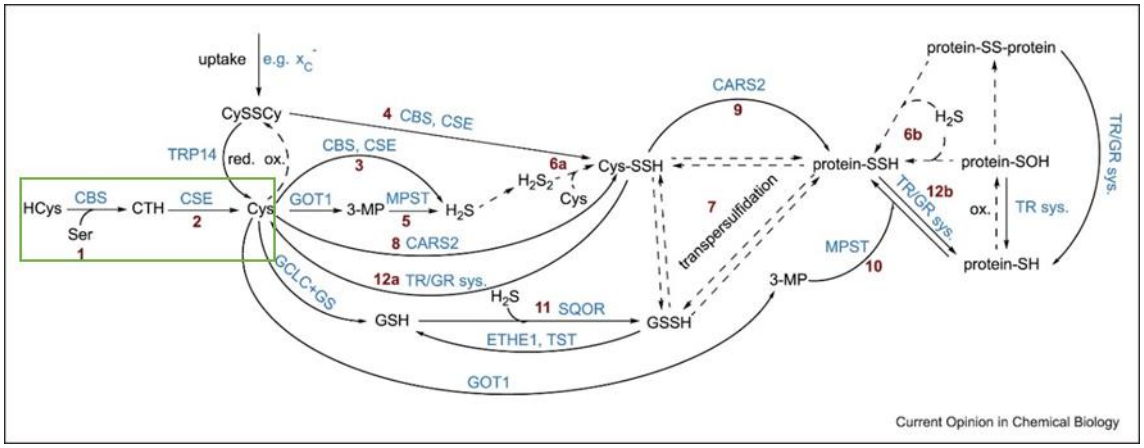

Figure 2. ***Metabolic pathways of RSS****, adapted from Versatile roles of cysteine persulfides in tumor biology (24). Plain arrows represent enzymatic reactions mediated by the indicated enzymes, while dashed arrows indicate non-enzymatic processes. The transsulfuration pathway is marked in green. Abbreviations on the figure not listed in the text: CySSCy: cystine, Cys: cysteine, Cys-SSH: cysteine-persulfide, 3-MP: 3-mercapto-pyruvate*

1.2.1 Low molecular weight persulfides

Beside their canonical reactions, Cbs and Cse can catalyze similar secondary reactions, by which play key roles in LMW RSS production, including H_2S and cysteine persulfide (CSSH) (25, 26) (reactions 3 and 4, respectively). While for producing H_2S, CSH is the source of sulfur; for direct CSSH formation, CSSC is used as the substrate (27). Under normal cellular conditions, due to the highly reducing environment, the CSH-to-CSSC concentration ratio favors CSH as a substrate and therefore H_2S production is more prevalent (25). However, under more oxidizing conditions, the drop in the CSH/CSSC ratio can make CSSC the preferred Cse/Cbs substrate to directly produce CSSH (10). CSSH can also be formed by cysteinyl-tRNA synthetase (Cars2), but this enzyme uses CSH rather than CSSC (reaction 8) (28). CSH can react with inorganic polysulfide species to produce LMW CSSH (reaction 6a), but this is a non-enzymatic process (29, 30).

The reduction of LMW CSSH is catalyzed by the Thioredoxin (TRP14/Trx/TrxR) and glutathione (GSH/GSSG reductase (GR) and glutaredoxin) systems (TR/GR), where the reducing equivalents from NADPH are converted to cleave the S-S bond (31, 32).

In cellular systems, the most abundant LMW persulfide is glutathione persulfide (GSSH). Recent studies have confirmed that GSSH has an important cellular function to protect against lipid peroxidation-induced ferroptosis (17, 18). The production of GSSH is catalyzed by Sulfide Quinone Oxidoreductase (SQOR) using H_2S and GSH (33-35). The catabolism of GSSH involves two enzymes, Ethylmalonic Encephalopathy 1 (ETHE1) and Thiosulfate Transferase (TST) (36). These enzymes, along with GSH and GSSH, constitute the primary machinery for H_2S catabolism (34).

1.2.2 High molecular weight persulfides

Protein persulfidation is a common posttranslational modification on protein thiol side chains. Persulfidation can regulate protein function: it can either activate or inhibit enzyme activity in a protein-specific manner (37, 38).

There are a dynamic equilibria between endogenous RSS, including the LMW and HMW presulfide species (39). For example, in a process called transpersulfidation, the outer sulfur atom of one persulfide can be transferred to another. This non-enzymatic process was proposed to play a significant role in protein persulfide formation, where a LMW persulfide (CSSH or GSSH) persulfidates a thiol protein, creating a P-SSH and a corresponding LMW thiol (reaction 7) (29, 40). Other non-enzymatic reactions that can generate persulfidated proteins (reaction 6b) are typically sulfide-mediated, where H_2S reacts with either a protein-disulfide (P-SS-P) or a protein sulfenic acid (P-SOH) (41, 42).

HMW persulfides can also be generated enzymatically via 3-mercaptopyruvate sulfurtransferase (MPST), which acts as a persulfide transferase. MPST uses 3-mercapto-pyruvate as a substrate to produce pyruvate while the enzyme itself becomes persulfidated (43, 44). In the next step, this persulfide moiety can be directly transferred to another LMW or HMW thiol (reaction 10) (29).

The above-mentioned processes are posttranslational modifications. A recent report proposed that persulfidated proteins can potentially be produced translationally, where

Cars2, can produce and incorporate CSSH into polypeptide chains and thereby produce persulfidated proteins inside the ribosome (reaction 9) (28).

HMW persulfides can also be reduced by the Thioredoxin (TRP14/Trx/TrxR), and glutathione (GSH/GSSG reductase (GR) and glutaredoxin) systems (TR/GR), where NADPH is again the source of reducing equivalents that cleave the S-S bond. This process restitutes the native thiol form of the protein (40) and produces H_2S.

Besides its modulating effects, persulfidation also protect proteins from irreversible oxidation, since the oxidized persulfide species (such as P-SSO_{2-3}) can be reduced along the S-S bond back to the active enzyme, unlike their oxidized thiol counterparts (37, 45). This process can become important under excessive oxidative stress e.g. in tumor cells, where ROS production is elevated (13, 24).

1.3 Chemical properties of RSS

RSS exhibit promiscuous redox activity (46), and sulfane sulfur plays a central role in defining their chemical behavior (47). RSS can participate in both 1-electron and 2-electron reactions and, in some reactions, can exhibit higher reaction rates than the corresponding thiols; therefore, they are sometimes called ‘hyperactivated thiols’(16).

In 2-electron reactions, per- and polysulfide species can act both as an electrophile and a nucleophile, depending on their protonated state and reaction partner (16). The protonated version (R-S_nS-H) is a potent electrophile because it can provide good leaving groups, such as HS-. However, at physiological pH, the preferred protonated state for most persulfide species is the deprotonated form (R-S_nS^-), because their pKa is lower than that of their thiol counterparts, which is caused by two factors. Delocalization of the negative charge along the sulfur chain stabilizes the anionic form, and the S-H bond is also weaker compared to the thiols (48-50). These forms are highly reactive towards electrophiles, making per/polysulfide species superior nucleophiles compared to the corresponding thiols (16). This phenomenon arises from the high polarizability of sulfur, known as the alpha-effect, whereby the lone pair electrons of the penultimate sulfur atom enhance the electron density at the terminal sulfur (48). As a result, persulfide anions are particularly reactive toward electrophiles, alkylating agents, and specific oxidizing species, such as hydrogen peroxide (H_2O_2); hence, oxidative stress typically leads to excessive production of oxidized per- and polysulfide species (13, 37, 45).

In addition, per- and polysulfide species are better radical scavengers than their thiol counterparts, because the unpaired electron can be delocalized through the sulfur chain (51). This makes the per/polysulfide species a good H atom donor. Homolytic cleavage also generates thiyl- and perthiyl radicals ($R\text{-}S_nS\bullet$), where the perthiyl is more stable, again because of electron delocalization. The ability of per/polysulfides to act as efficient radical scavengers, thereby generating more stable intermediates, reflects the broad reactivity and biological promiscuity of RSS (52, 53).

Persulfides can also undergo heterolytic cleavage or participate in disproportionation and comproportionation reactions to induce interconversion via sulfur exchange, resulting in a wide variety of sulfur species with different sulfur chain lengths. These interconversions that occur between RSS via dynamic equilibrium processes constitute the so-called RSS pool (28, 46, 54). Equilibria can be shifted by many factors, like changes in the redox environment.

As a consequence, the RSS pool is highly sensitive to the cellular redox environment, enabling RSS to function as redox switches, because the oxidized forms (disulfides, persulfides, sulfenic acids, sulfinic acids) participate in distinct reactions with different biological roles compared to the corresponding thiols (2, 27, 32, 37, 55, 56). Due to these chemical properties, RSS can rapidly react with a wide variety of biomolecules in a cellular milieu and, therefore, are considered as biologically labile species. This is why their endogenous detection requires careful control of experimental conditions.

1.4 Detection of RSS

It is important to have robust methods that can measure dynamic changes in the levels of RSS in order to get deeper insights into their biological roles. As explained above, this is complicated by the fact that RSS constitute a dynamic interconnected system (Figure 2). Therefore, it is beneficial to measure as many RSS as possible at the same time. However, their high reactivity and labile properties make detection challenging (57-59). Hence, it is essential to start the detection protocols by “freezing” their dynamic equilibria by converting them into stable and detectable forms, while maintaining cellular speciation.

A non-specific approach in the literature for RSS quantification is the utilization of sulfane sulfure probes (e.g., SSP4 (52), DSP-3, or pyronine-based FRET fluorophores (60, 61)). These are natively non-fluorescent compounds that react with sulfane sulfur to

produce fluorescein, a highly fluorescent molecule that can be detected with a fluorescent plate reader. For example, the use of SSP4 provides information about the sulfane sulfur pool in cells (62), but cannot distinguish between any of the sulfane sulfur species, not even between LMW and HMW species.

Apart from live-cell imaging techniques, the first step in most analytical methods for RSS detection is cell or tissue lysis. During this step, changes to the persulfidome can be induced. Therefore, it is important to thoroughly investigate this effect because, in the case of inefficient alkylation, it can seriously disturb the distribution of RSS (57, 63, 64).

1.4.1 Alkylation-based detections

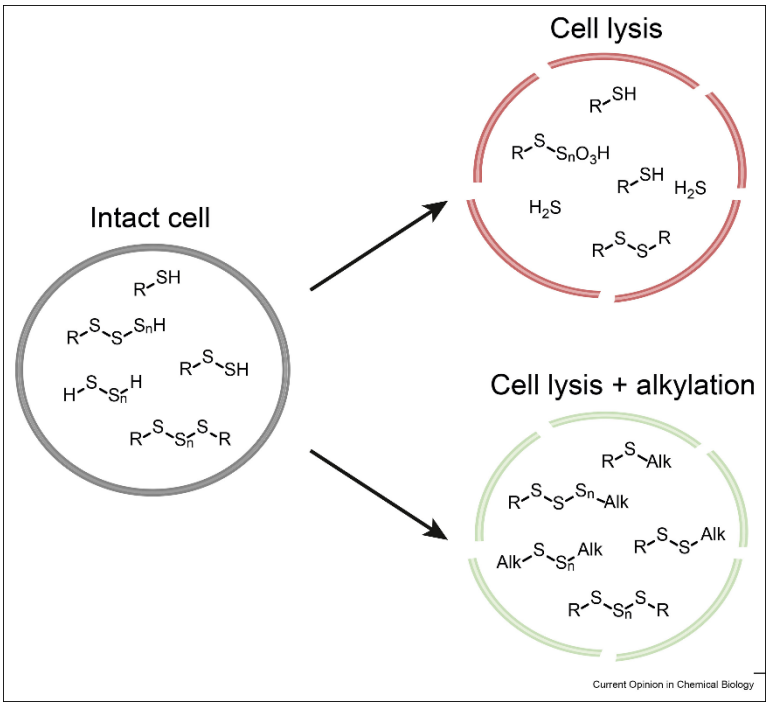

Figure 3. ***Alkylation is anticipated to maintain RSS speciation during cell lysis****. Without alkylating agents, cell rupture tends to promote different oxidation, reduction, and interconversion reactions, leading to modifications and changes in speciation (upper right). Using alkylating agents, hydroper/polysulfides are expected to be preserved for analysis as stable, alkylated species (lower right). Figure adapted from The influence of alkylating agents on sulfur-sulfur bonds in per- and polysulfides (59).*

Alkylating agents are used to stabilize RSS as alkylated, labeled derivatives (e.g., R-S-Alk., R-S_nS-Alk.) (59, 63). Alkylating agents react with per- and polysulfide species as well as with thiols (63). Due to differences in reaction rates, it is important that the

alkylation of all species is faster than any other lysis induced reaction. Alkylation-based methods can be grouped in 3 subgroups based on their chemical features.

I) Selective labeling: Selective alkylating agents are used, like S-methyl methanethiosulfonate (MMTS), which was claimed to be "thiol-specific" or dimedone-based probes that react specifically with sulfenic acids. (42). Alternatively, the different reactivity of thiols and persulfide species may be exploited: at low pH, thiols can be protonated, while persulfide species remain anionic. Since the alkylating agent will only attack the anionic forms, it is assumed that only the persulfide species are labeled (65).

The selectivity of these methods is limited; specific alkylating agents can artificially shift chemical equilibrium and therefore their use is not recommended (57). MMTS also labels persulfide species. In the low pH method, thiols with low pKa values may also be labeled; additionally, persulfide alkylation may remain incomplete; however, applying longer alkylation times will result in the alkylation of thiols with higher pKa values due to slowly shifting protonation equilibria.

II) Tag-switch-based methods: In these protocols, the alkylating agent labels all thiol and per/polysulfide species (R-S-Alk. R-S_nS-Alk., respectively). Next, the tag from the per/polysulfide species is selectively removed. This could occur via S-S bond reduction (32, 38, 66) or by a direct tag-switch (45, 67, 68).

These methods are suitable for immunoblotting and proteomic approaches; however, non-selective labeling of amines and other reactive functional groups can lead to false-positive/negative signals. Additionally, LMW persulfide are lost during the sample preparation.

III) High Performance Liquid Chromatography (HPLC) separation: Since most alkylating agents can and will react with both thiol and per/polysulfide species, it is now widely accepted that selective labeling is not an effective approach. However, HPLC can separate the different alkylated species (28, 37, 69-71).

This methodology enables distinguishing LMW and HMW persulfide species and permits the individual quantification of per- and polysulfides. However,

it requires an HPLC machine, preferably coupled with a Mass Spectrometer (MS).

For metabolomic analyses, HPLC-based separation methods are the most suitable.

1.4.2 The choice of alkylating agent

Alkylation is a fundamental step in most detection protocols. There is a variety of alkylating agents that can be used to capture thiols; however, the choice of alkylating agent is crucial, as some of them can destabilize per- and polysulfides, initiate sulfur loss, and yield alkylated thiols instead of the derivatized per- and polysulfides (57-59). This can lead to an underestimation of the persulfidome.

In polysulfide species, the sulfur loss can occur through S-S bond cleavage by electrophile-assisted hydrolysis, where the alkylating agent can be attacked by a lone pair electron of a mid-chain sulfur. In the case of persulfide species, tautomerization can be the main reason for sulfur loss: it converts to the corresponding thiosulfoxide, and a sulfur can be lost upon further attack by the alkylating agent (58).

As stated before, it is vital to ensure that the alkylating agent reacts faster with all sulfhydryl groups in the sample compared to any lysis-induced or interconversion reactions; otherwise, alkylating agent induced shifts in chemical equilibria can alter RSS speciation and give artifactual results.

These effects are more relevant in the case of N-ethyl maleimide (NEM) (57) and less prevalent with the iodoacetamide (IAM) derivatives, especially with (β-hydroxyphenyl)ethyl iodoacetamide (HPE-IAM). The reason behind this is the observation that alkylating agents that contain a phenol moiety have been proven to have an S-S bond protecting or stabilizing effect and can preserve persulfide species. However, the mechanism behind this phenomenon remains unknown (70, 72).

Because they preserve reactive per- and polysulfides, IAM derivatives, especially HPE-IAM, are a favorable choice of alkylating agent for per- and polysulfide-centric metabolomic approaches (28, 70, 72). HPLC separation, followed by ultraviolet-visible (UV-Vis) or MS detection, is the preferred technological setup for the simultaneous quantification of small-molecule RSS. Furthermore, MS-based methodologies enable the

utilization of stable isotope labeling and fluxomic approaches, permitting time-resolved analyses.

1.5 Utilization of the HPE-IAM based detection protocol to investigate the roles of RSS in biological systems

1.5.1 Roles of the transsulfuration pathway in maintaining CSH homeostasis in liver hepatocytes lacking the thioredoxin and glutathione based reducing systems

The two primary disulfide-reducing systems within the cells, the Trx and GSH systems, use NADPH to fuel their disulfide-reducing capacities. Co-disruption of these two vital reducing systems is lethal in bacteria and yeast, but genetically engineered mouse models, in which livers lacking both thioredoxin and glutathione reductase, thrive; this mouse model was first reported in 2015 by Eriksson et al. (73). Interestingly, these mice developed increased sensitivity to inhibition of either GSH synthesis or the transsulfuration pathway (73), CSH produced by the transsulfuration pathway is vital under these conditions. In a recent study, we demonstrated using the HPE-IAM based RSS detection protocol that TRP14, a unique member of the thioredoxin system, is the enzyme that is directly responsible for CSSC disulfide bond reduction under normal conditions. And this is the primary pathway for CSH production from CSSC via xCT (22). However, TRP14 activity requires intact TrxR activity, and we uncovered that under conditions in which both the Trx and GSH systems are disrupted, transsulfuration becomes essential in these livers. Previously, we thought that transsulfuration is responsible for CSH production using Met+Ser, via the canonical activities of the transsulfuration enzymes. In our recent study, which is the main article of my PhD thesis, we demonstrated that transsulfuration produces CSH via a unique secondary activity of the transsulfuration enzyme, Cse (74). This mechanism is discussed in detail in the Results section.

1.5.2 Roles of RSS in tumor progression

Our research group is primarily focused on the secondary activity of the transsulfuration enzymes, Cse and Cbs, which produce RSS as shown in the previous section. We are particularly interested in the roles of these RSS in tumor progression. Throughout the years, we demonstrated that RSS play different roles in different tumor types.

In another study, we demonstrated that the RSS produced by the transsulfuration enzymes plays a crucial role in tumor progression in basal-like breast cancer, where the Cbs is overexpressed. We demonstrated that Cbs can protect these cells from oxidative stress and CSH starvation–induced ferroptotic cell death. We also showed that genetically modified cells, in which Cbs was silenced, were more susceptible to CSSC deprivation and oxidative stress. In these Cbs silenced cells, Cse, the other transsulfuration enzyme, was overexpressed. The susceptibility to CSSC starvation and the increased activity of transsulfuration enzymes suggested that, in addition to their canonical function, the secondary enzyme functions also play a crucial role in tumor progression. Additionally, we confirmed that the inhibition of both transsulfuration enzymes significantly reduced tumor growth in xenograft models (11).

In another study, we showed that in BRAF V600E melanoma, the transsulfuration pathway realigns in response to drug treatment and plays a key role in the development of drug resistance. In response to the treatment, Cse is upregulated, whereas Cbs is downregulated; however, in resistant cells, Cbs becomes more abundant, while Cse expression and activity decrease. In this context, we also verified that this effect is induced by the secondary, RSS-producing functions of the transsulfuration enzymes, rather than by their canonical functions. Furthermore, we validated that inhibiting Cse can delay the development of drug resistance (10).

Another biological system in which I utilized my methodology was pancreatic ductal adenocarcinoma (PDAC) progression. Cbs produced RSS are involved in metastasis formation via orchestrating epithelial-to-mesenchymal transformation (EMT) through Wnt signaling. During my doctoral studies, I participated in measurements within these investigations. In this tumor type, Cbs was also overexpressed so we investigated how this enzyme promotes PDAC tumor progression and metastasis formation in a translational research project (12).

2 Objectives

Reactive sulfur species (RSS) are crucial regulators of cellular functions and intracellular redox balance; however, their inherent chemical instability makes their reliable detection technically challenging. The main goal of my PhD research was to optimize and implement an analytical platform for detecting RSS to better understand their metabolism and biological significance under different conditions. To gain a deeper understanding of their dynamic metabolism and interconversion, we developed and performed time-resolved fluxomic analyses in different biological systems.

My first aim was to critically re-evaluate and optimize our current RSS detection protocol, focusing on the key parameters that can influence the reproducibility and reliability of our data, with a special focus on preserving the presulfide species.

My second objective was to apply the optimized method to various biological matrices, including cultured cells, tissue samples, and cell-free plasma, for comprehensive RSS monitoring and to further improve and expand the analytical method to enable time-resolved fluxomic analyses and use this technique to study the metabolism and catabolism of selected RSS and to track their dynamic fluctuations over time in *in vitro* systems.

With the optimized RSS detection protocol, I aimed to investigate the metabolic pathways of RSS in two complex biological systems. In a genetically engineered mouse model in which the livers lack both the Trx and GSH machineries, my objective was to identify the origin of cysteine and assess the contribution of the different cysteine-producing pathways maintaining the redox homeostasis.

The methods that I optimized were also used to explore the roles of protein persulfide species in the formation of pancreatic ductal adenocarcinoma (PDAC) progression and metastasis.

3 Methods

3.1 Reagents and standard protocols

All reagents and chemical compounds were high-grade products purchased from Merck, Sigma, and VWR. All amino acids used were the L-enantiomers. All metabolomic and fluxomic data are normalized to total protein content, and the mean and SD are shown, except where individual points are displayed.

3.1.1 Isotope-labeled amino acids

[$^{13}C_6$,$^{15}N_2$]-cystine was purchased from Cambridge Isotope Laboratory (catalog CNLM-4244-H-PK). For [^{34}S] amino acids, an in-house synthesis and purification protocol was established (Miller, Austad, Prigge, and Schmidt, unpublished).

3.2 Cell culture

For method optimization Cal51 cell line was used. Cells were maintained in a 5% CO_2 incubator at 37°C in RPMI 1640 media supplemented with 10% fetal bovine serum (FBS), 2 mM L-glutamine, 100 U/ml penicillin/streptomycin (Pen/Strep), and 100 nM sodium-selenite.

3.2.1 Lentiviral transduction

For HMW persulfide studies, the PDAC T3M4 cell line was used, and lentiviral transduction was carried out. A lentiviral-mediated gene-specific shRNA system (Sigma, St. Louis, MO, USA) was used for creating stable knockdown. Cbs-specific particles were MISSION shRNA Lentiviral Transduction Particles (SHCLNV-NM_000071, ID: TRCN0000291407). An empty vector (MISSION pLKO.1-puro, SHC001V) was used as a control transduction particle. Lentiviral particles were administered at a multiplicity of infection (MOI) of 5. Following a 48-hour transduction period, cells were selected with 5 μg/mL puromycin for 48 hours, and the process was repeated twice. Single-cell colonies were established by seeding 1 cell per well into 96-well plates, upon colony formation, they were transferred to 24-well, 12-well, and 6-well plates, respectively.

3.3 Metabolomic and fluxomic analyses

3.3.1 Sample preparation for cells and tissue samples

Thiol and persulfide species were alkylated with β-(4-hydroxyphenyl)ethyl iodoacetamide (HPE-IAM), based on the published method by Akaike et al.(28). Briefly,

the cells were scraped in 75% methanol (MeOH) containing 5 mM HPE-IAM or the cryopulverized tissue samples were resuspended in it. After sonication, the samples were alkylated at 37°C for 20 min and centrifuged (14 000g; 10 min; 4°C) to remove precipitated protein. The supernatant was acidified with 10% formic acid (FA) and diluted with eluent A (0.1% FA in water) before injection. The samples were kept on ice between each step. The remaining pellets were resuspended in 1% SDS/PBS, sonicated and protein content was measured by BCA assay.

3.3.2 HPLC-MS/MS method

The high-performance liquid chromatography-tandem mass spectrometry (HPLC-MS/MS) measurements were carried out on a Thermo Vanquish UHPLC (ultra-high-performance liquid chromatograph) coupled with a Thermo Q-Exactive Focus Orbitrap MS. Positive ionization mode and higher-energy collisional dissociation were used to detect the metabolites (specified in Table 1).

Table 1. ***Detected masses and fragmentation for the examined analytes****. The mass for the thiol and persulfide species is the HPE-IAM derivatives. Thioethers and disulfides are detected in their native, protonated form. The isotopically labeled species are indicated (74).*

Analyte	Precursor (m/z)	Fragment (m/z)
Alkylated compounds		
CSH	299	121
[^{34}S] C**S**H	301	121
[$^{13}C_3$,^{15}N] CSH	303	121
CSSH	331	121
[^{34}S] CSSH	333	121
[^{34}S,^{32}S] C**S**SH	333	212
[^{32}S,^{34}S] CS**S**H	333	214
[$^{34}S_2$] C**SS**H	335	121
[$^{13}C_3$,^{15}N] CSSH	335	121
GSH	485	356
[^{34}S] G**S**H	487	358
[$^{13}C_3$,^{15}N] GSH	489	360
H_2S	389	252

[^{34}S]H_2**S**	391	254
Disulfides and thioeters		
CSSC	241	152
[^{34}S,^{32}S] C**S**SC	243	154
[$^{34}S_2$] C**SS**C	245	156
Cth	223	134
[^{34}S] Cth	225	136
GSSG	307	130
[^{34}S,^{32}S] G**S**SG	308	130;131
[$^{34}S_2$] G**SS**G	309	131

The alkylated thiols and persulfides were analyzed on a Phenomenex Kinetex C18 (50 x 2.1 mm, 2.6 µm) column, eluents 0.1% FA/H_2O (A) and 0.1% FA/MeOH (B). In the original gradient, 5% B was linearly increased to 95% in 15 min, then back to 5% in 2 min; the flow rate was 0.3 ml/min, 30°C. In the modified gradient, the initial 5% B was increased to 13%, then to 95% in 2 and 4 min, held there (0.5 min), and back to 5% in 0.1 min. The flow rate was 0.5 ml/min and the column temperature was 40°C.

Thioether and disulfides were measured on a Thermo Scientific Hypercarb (100 x 2.1 mm, 3µm), with eluents of 0.5% FA/H_2O (A) and 0.5% FA IPA: ACN 1:1. (B). The gradient was as follows: 0% B increased to 3% in 1.5 min, to 30% in 3.5 min, then to 100% in 1 min, held there for 2 min, and back to the initial 0% in 1 min. The flow rate was 0.2 ml/min, and the column was maintained at 40°C.

3.4 Mouse experiments

All mouse protocols were reviewed and approved by the Montana State University Institutional Animal Care and Use Committee (MSU IACUC; approval numbers 2018-118-01, 2019-50-97, 2021-118-01, 2021-118-IA, 2022-50-IA, or 2023-225-IA) or the University of Veterinary Medicine Budapest, Hungary (UVMB), Animal Research Ethics Committee (approval numbers PE/EA/00744-6/2022 and PE/EA/00977-6/2023). All mice were kept in forced-air HEPA-filtered caging systems and were specific pathogen-free (SPF). All mouse harvests were performed between 9:30 and 11:30 to minimize the circadian effects; experimental mice were 8 weeks to 8 months old.

TR/GR-null mice are full-body knockouts for glutathione reductase (GR) and liver-specific disruption of TrxR1 and Trx.

3.4.1 Jugular catheterization and stable isotope administration

Jugular catheters, harnesses, and swivels were installed following the general procedures outlined, as modified in accordance with recent publications or our experience (Seaford, Miller, Austad, Noyd, Juranyi, Nagy, Schmidt; unpublished).

Stable isotope-labeled amino acids were administered through a jugular catheter at a flow rate of 2 µl/min for 4 hours, with a concentration of 10 mg/ml (total 4.8 mg labeled amino acid/mouse). The labeled amino acids were dissolved in saline, except for labeled CSSC, which was dissolved in 175 mM HCl.

3.4.2 Inhibitor treatments

We utilized AOAA or PAG to evaluate the role of Cbs and Cse *in vivo*. To test the inhibitor effect on resting liver metabolites, mice received IP injections of 0.5 ml AOAA or PAG (10 mg/kg) in sterile saline 4 times hourly, and were harvested at hour 5.

In the stable-isotope labeling experiment, mice received a single IP dose of AOAA (5 mg/kg) 15-30 min before the infusion, during which the infusate also contained AOAA (5 mg/kg, for a total of 10 mg/kg). Mice showed no overt adverse effects in either experiment.

3.5 Primary hepatocytes

3.5.1 Isolation of primary hepatocytes

The isolation method was carried out as published previously (75). Briefly, anesthetized mouse's portal vein was cannulated and infused with perfusion buffer (PBS, 0.5 mM EGTA, 25 mM HEPES, pH 7.6, 3.7 mg/ml sodium bicarbonate, 1.1 mg/ml glucose). After that 10 ml of digestion solution was added (150 mM NaCl, 5 mM $CaCl_2$, 0.3 mM $ZnSO_4$, 5 mM HEPES pH 7.6, 3.7 mg/ml sodium bicarbonate, 1.1 mg/ml glucose, 0.413 mg/ml Type IV collagenase [Sigma-Adrich C1538], 0.13 mg/ml Liberase [Roche 853898], 0.1 µg/ml DNAse I [Sigma-Adrich#DN25]). Upon initiating infusion, the inferior vena cava was cut for outflow. The liver was then placed in a culture dish with HBSS and Pen/Strep and incubated (37°C, 5% CO_2) for 10 min. After rinsing and changing the HBSS, the fine surface tegument surrounding each lobe was gently peeled away. The

released hepatocytes were filtered (70 μm nylon) on ice to ice-cold DMEM supplemented with Pen/Strep, pyruvate, glutamine, selenite (hereafter "SF-DMEM"), 10% FBS, and gelatine. The hepatocytes were rinsed 3 times with SF-DMEM. To sediment the hepatocytes, the tube was gently mixed and centrifuged (4°C, 300 g, 3 min) 4 times. After that, cells were plated onto collagen-coated 6-well culture dishes. SF-DMEM was changed 90 min and 1 day after plating to remove the excess hepatocytes. Cells were used on days 1-4 post-isolation.

3.5.2 Fluxomic analyses

For fluxomic analyses, serum-free Met/CSSC-free DMEM (Thermo Fisher#21013024) was used, supplemented with [^{34}S]-labeled or unlabeled Met and CSSC; the final concentrations matched those of the normal DMEM (200 μM each). The medium was also supplemented with 2 mM L-glutamine, 100 U/ml Pen/Strep, pyruvate (1mM) and 100 nM sodium-selenite.

Cells were washed before media change, and the sample preparation was carried out as described in 4.2. section. For inhibitor studies, the cells were pre-treated with the inhibitor (1 mM) for 24 h before adding the labeled media.

Cells were lysed in 5 mM HPE-IAM conaining 75% MeOH, and the alkylation and HPLC-MS/MS analyses were carried out as described above. Labeled and unlabeled analytes were measured as indicated and the labeling ratios were calculated.

3.6 *In vitro* biochemical reactions

3.6.1 Liver lysate experiments

Biochemical reactions were based on published assays on recombinant Cbs and Cse activity assays (25, 76) adapted for liver lysates with the following modifications: cryohomogenized liver powder was rehomogenized in lysis buffer (50 mM HEPES, pH 7.4; 150 mM KCl; 0.1% CHAPS, protease inhibitor cocktail [Sigma 04693159001]), sonicated and centrifuged (14 000g, 10 min, 4°C). Protein concentration was measured by the BCA assay kit. The final protein concentration was 2-4 mg/ml.

The lysate samples were kept on ice, and PAG was added prior to the initiation of the reaction at a final concentration of 1 mM. For the lysates, a 10x MasteMix (5 mM [$^{34}S_2$]-CSSC, 2 mM PLP, and/or 1 mM NADPH) was added, and the mixture was incubated at

25°C to complete the reaction. After 30 min, the reaction was stopped by adding ice-cold 75% MeOH containing 5 mM HPE-IAM, and the alkylation and HPLC-MS/MS analyses were carried out as described above.

3.6.2 Recombinant Cse reaction

The recombinant Cse (0.5 μM) reaction was carried out in the same buffer as described above. The protein was kept on ice, and 10x Master Mix (2 mM PLP and 5 mM [$^{13}C_6$, $^{15}N_2$]-CSSC) was added, then the mixture was transferred to 25°C, and samples were taken at the indicated time points. Ice-cold 75% MeOH containing 5 mM HPE-IAM was added to stop the reaction; the alkylation and metabolomic analyses were carried out as described above.

3.7 HPLC-MS/MS measurements for protein persulfides

To detect protein persulfides, cells were scraped in RIPA buffer containing 5 mM HPE-IAM. After sonication and centrifugation (14 000g, 10 min, RT) supernatants were desalted with spin columns (Zeba spin columns, 7K MWCO, 0.5 ml). Protein content was measured in the flow-through using the BCA assay. 100 mM HPE-IAM in DMSO was reintroduced to the samples, and protein concentration was brought to 1 mg/ml. For digestion, pronase (final concentration: 3 mg/ml) was used in a 35 mM Na-acetate buffer (pH 5.0) at 37°C for 1h 10% trichloric acid was added, and the undigested proteins were precipitated. The HPLC-MS/MS method for cysteine and cysteine-persulfide were the same as described in section 4.2.2.

3.8 Statistical analyses

Statistical analyses and graphical representation were performed with GraphPad Prism software. Student's T-test was used for pairwise comparisons for all figures, unless indicated otherwise. For liver lysate experiments, one-way ANOVA with Tukey's correction was used. Significance was assigned as * for $p < 0.05$; ** for $p < 0.01$, $p > 0.05$ is indicated as ns (not significant, $p > 0.05$), where it is relevant.

4 Results

4.1 Systematic optimization of the HPE-IAM based RSS detection protocol

Initially, I focused on the alkylation protocol (Figure 4) and carefully and systematically investigated and revised critical reaction parameters. We used the alkylating agent that was specifically recommended for persulfide detection: the iodoacetamide derivative HPE-IAM, which was shown to protect against polysulfide chain cleavage upon the alkylation process (72).

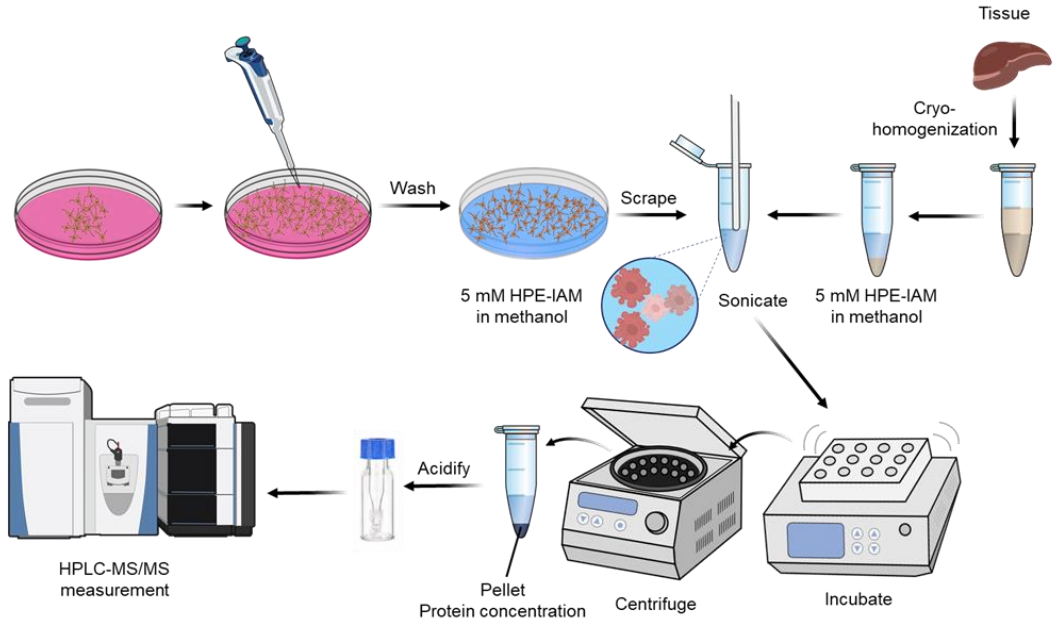

Figure 4. ***HPE-IAM based sample preparation from cells and tissue.***

4.1.1 Scraping cells on ice can prevent persulfide species from degradation

The initial stage of the sample preparation procedure involves collecting the cells, which, for adherent cells, is achieved by scraping them off the plate. We examined the effect of temperature on this step to minimize the decay of labile persulfide species and any unwanted enzymatic reactions in the cells. Cells were washed, then an HPE-IAM-containing ice-cold methanol solution was added, and scraping was performed either on ice or at room temperature.

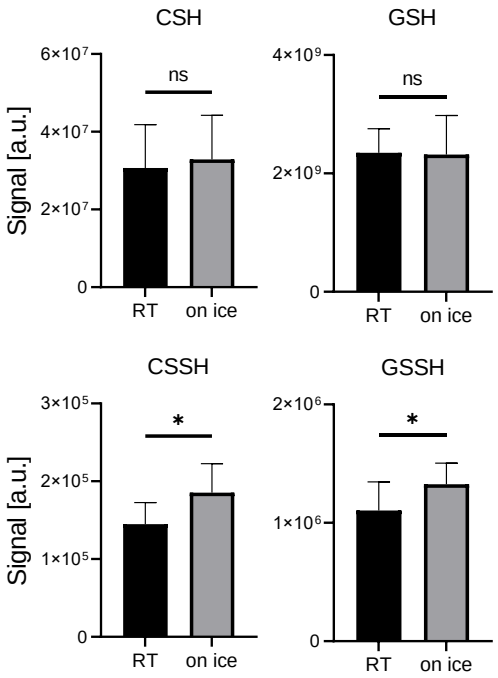

Figure 5. ***The impact of temperature during cell scraping.*** *Cal51 cells were scraped either at room temperature (RT) or on ice and the HPE-IAM based alkylation method protocol was performed; levels of cysteine (CSH), glutathione (GSH), and their persulfide derivatives (CSSH and GSSH, respectively) were measured. Mean (n=9) and S.D. are shown. Unpaired, two-sided t-test was used, where ns (not significant) p>0.05, * p<0.05, ** p<0.01.*

Temperature during the scraping process had no effect on thiol species (CSH and GSH, Figure 5, upper panels), but higher levels of LMW persulfides (CSSH and GSSH, Figure 5 lower panels) were detected when the process was performed on ice, suggesting that lower temperature may preserve persulfide species and may also reduce the evaporation of the lysis solution (MeOH).

4.1.2 Cell confluency at the time of harvest influences persulfide levels

We investigated the effect of cell confluency on the detected sulfur metabolome. Different cell numbers were plated to have different confluencies at harvest: subconfluent, confluent, and overly confluent ($2x10^5$; $4x10^5$; $8x10^5$ cells/ml in a 6-well plate).

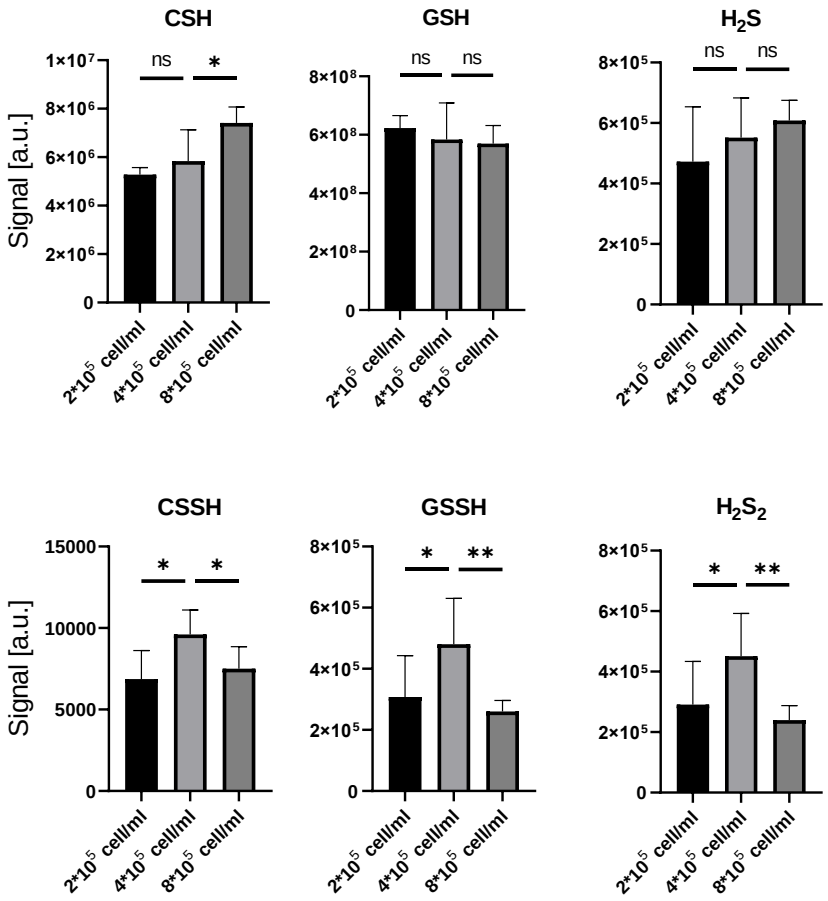

Figure 6. ***The effect of cell confluency on intracellular RSS species****. Different cell numbers of Cal51 cells were plated into 6-well plates the day before harvest, and the HPE-IAM alkylation protocol was performed the following day. Mean (n=4), and S.D. are shown, ns (not significant) p>0.05, * p<0.05, ** p<0.01.*

The data was normalized to protein content to gain comparable results. As shown in Figure 6, cell confluency has a significant effect on detected persulfide levels but not on thiol levels. The overly confluent cells had lower levels of persulfides and hydrogen disulfide. This effect is more likely a biological than a technical phenomenon; nevertheless, it shows that it is important to maintain the same confluency throughout the experiments.

4.1.3 Tight control of the alkylation parameters is required to gain reliable and reproducible results

At standard alkylating agent concentration conditions, temperature and time are the two main parameters that can affect the alkylation process. We indeed found that systematic optimization of these parameters is necessary for reliable and reproducible sulfur species detection. We performed time-dependent analyses at different temperatures and monitored the changes in the levels of alkylated species; the results are shown in Figure 7.

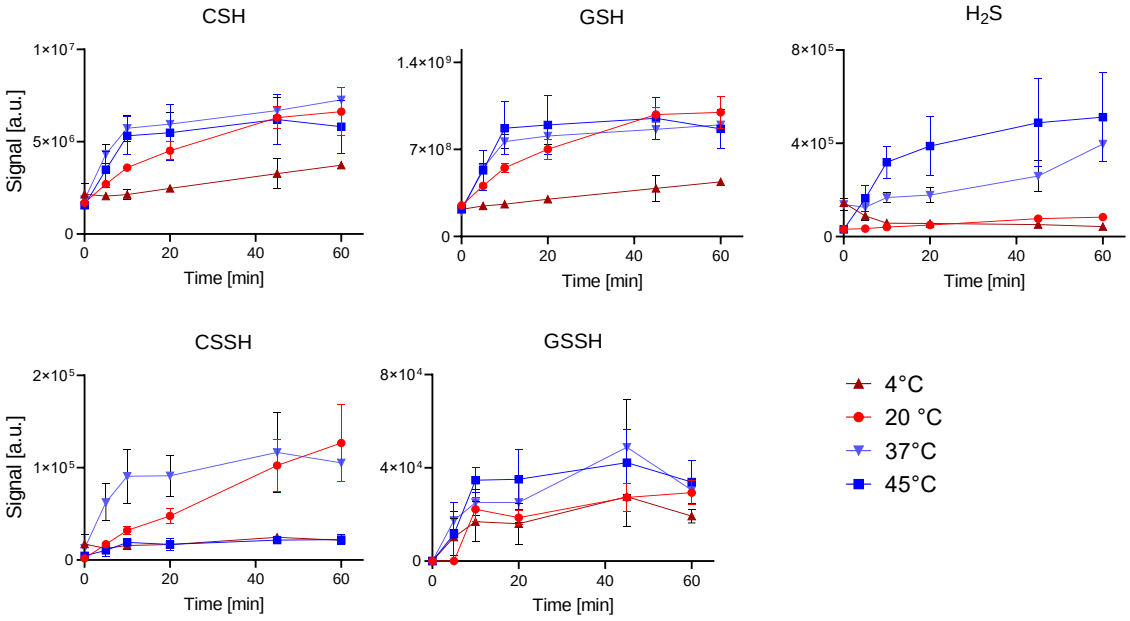

Figure 7. ***The influence of the alkylation parameters*** *(time and temperature). Time-dependent analyses were performed, and the levels of the specified alkylated species were measured at intervals of 0, 5, 10, 20, 45, and 60 minutes.*

In the case of thiols (CSH and GSH), at higher temperatures (37°C and 45°C), the alkylation reaction appeared to be faster than at 20°C. At 20°C, the alkylated thiols reach saturation after 45 min, but at higher temperatures, it occurs after 20 min. H_2S represents an exception; it doesn't reach saturation after even 60 min at 45°C and continues to increase. This is a result of a slow release of H_2S from the so-called sulfide pool, e.g., protein-bound sulfur (77). This correlates with the observation that at 20°C, the detected amount of alkylated H_2S is negligible. Therefore, the detection protocol of H_2S requires

a tight control of the alkylation time and at least 37°C, as our group showed in a previous systematic study (77).

Examining CSSH levels revealed a different pattern. At 4°C and 45°C, the amounts were low; we infer that at 4°C, alkylation is hindered and does not reach completion, whereas at 45°C, a temperature-induced degradation occurred. This experiment also revealed that at 4°C, the amount of alkylated analytes remained low even after 60 min, likely due to incomplete alkylation under the applied conditions. This suggests that keeping the samples on ice hinders alkylation.

Together, these data led us to conclude that 37°C and 20 min are the optimal alkylating parameters, but tight control of these parameters is required to achieve reproducible results.

4.1.4 Monitoring RSS levels with the optimized protocol during sample preparation

This experiment shows the entire sample preparation protocol to validate previous experiments, which were dedicated to parameter optimization. Scraping, as we have shown, is ideal at 4°C to prevent artificial reactions from occurring; then, samples need to be heated to 37°C for efficient alkylation of the sulfhydryl functional groups. Acidification efficiently stops the alkylating process by forming protonated thiols and persulfides, which are not susceptible to electrophile alkylating agents. Alkylated samples can be stored on ice (4°C) for an extended period of time, which can be achieved in the HPLC sample holder module.

These experiments corroborate that reproducible and comparable detection of RSS can be achieved under these experimental conditions.

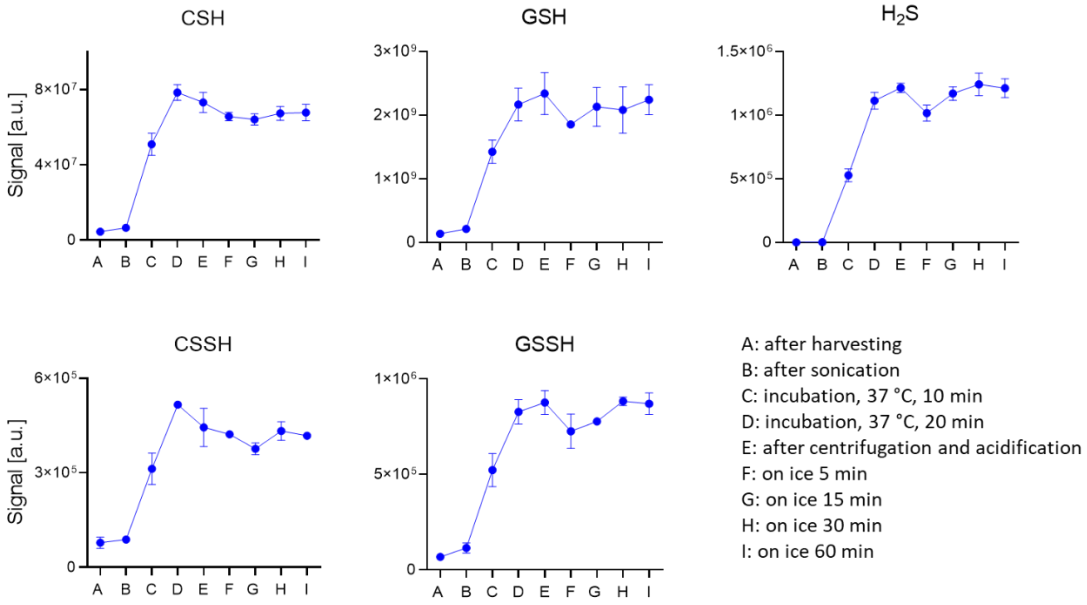

Figure 8. ***Alkylated species were monitored throughout sample preparation****. Cal51 cells were scraped in a 5 mM HPE-IAM containing MeOH solution. Samples were taken at the indicated steps, acidified, and the amounts of alkylated thiols and persulfides were measured by HPLC-MS/MS.*

4.1.5 Optimization of the HPLC-MS/MS method

A reverse-phase HPLC method can be used to separate HPE-IAM labeled thiol and persulfide species. The mobile phases are 0.1% FA in water (A) and 0.1% FA in MeOH (B). The initial protocol used a linear gradient beginning at 5% B eluent and increasing to 95% B, as shown in Figure 9A. We optimized this HPLC method to minimize the time of analysis. The original linear gradient was replaced with a two-step gradient, with a shallower phase, to maintain consistent initial steepness for the low-retention-time analytes, CSH and CSSH. This was followed by a steeper gradient. With this modification, retention times were reduced, and the analysis time decreased by half, from 20 min to 10 min. The gradients and typical chromatogram of the original methods are shown in Figure 9B.

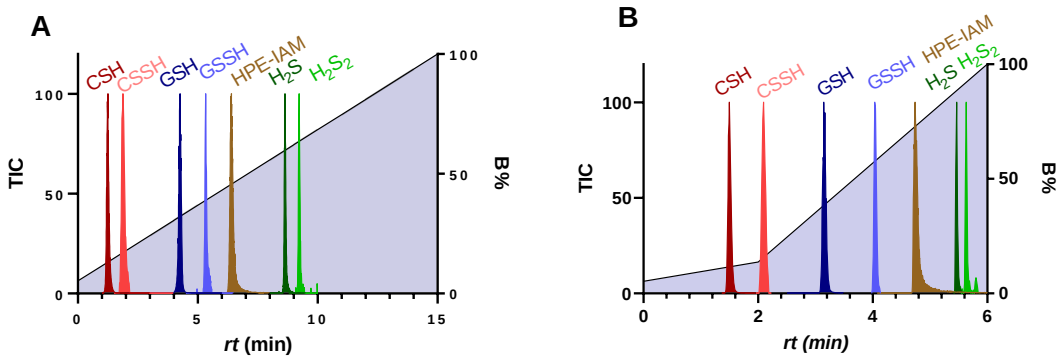

Figure 9. ***A typical chromatogram of the original (A) and the optimized (B) HPLC method.*** *On the left axis, the percent of eluent B (0.1% FA in MeOH) is indicated. TIC: total ion chromatogram*

The optimization doubled the method's throughput while maintaining baseline separation. This is important because it allows reduction of the time the samples need to spend in the autosampler to be reduced, thereby reducing the risk of degradation.

4.1.6 Mass spectrometry-based detection enables stable isotope tracing and fluxomic analyses

The optimized methodology permits the analysis of a greater number of samples and the gain of reliable data on labile species. Utilizing mass spectrometry-based detection enables the application of stable-isotope labeled amino acids for tracking metabolic fluxes in living cells and animal models. By employing stable-isotopically labeled amino acids, it is possible to investigate the activity of metabolic pathways both *in vitro* and *in vivo*. The labeled amino acids are administered to mice or intact cells, and the labeled analytes are subsequently quantified in a time-resolved manner. Changes in the quantity of labeled substrates and products indicate the activities of specific enzymes or pathways, whereas ratios of labeled to total (labeled/total) analytes reflect the relative activities of metabolic pathways.

Our group is primarily interested in metabolic fluxes through transsulfuration pathways, which can be followed by administering isotopically labeled substrates of the transsulfuration enzymes (e.g., Met, HCys, CSSC, and Ser, shown in Figure 2). One of the critical pathways that we are investigating is the catabolism of the CSSC taken up by xCt in cells. To follow CSSC metabolism, either carbon, nitrogen, or sulfur labeled analytes can be used. To gain deeper insight into persulfide (especially CSSH) metabolism, sulfur labeling is preferred, but the availability of sulfur-labeled CSSC is

limited; therefore, our group developed a synthesis method by which we produced the required amounts of this compound for our experiments.

This way, we can follow the metabolism of either the carbon backbone (by nitrogen and carbon labeling) or the sulfur (by using sulfur labeled CSSC). The most exciting analyte in our studies was the CSSH, which, in the case of the sulfur labeling, manifested in 4 different detectable species in the biological sample; i) unlabeled, ii) both sulfur labeled, and iii) only one sulfur labeled, where, based on the fragmentation patterns, we could separate whether the labeling was on the inner or the outer sulfur. Figure 10 depicts the different masses and fragmentation-based differentiation of one-sulfur labeled CSSH species.

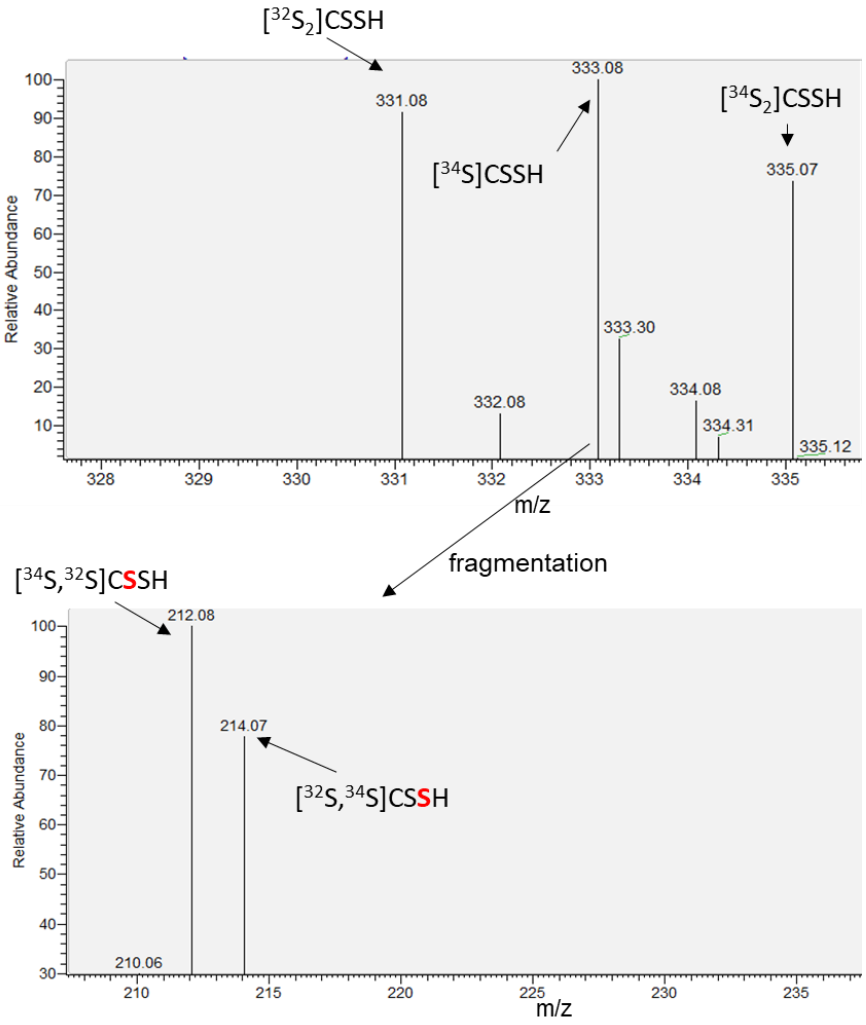

Figure 10. ***Mass spectra of the different CSSH species in experiments using [$^{34}S_2$]-CSSC labeling.*** *The three indicated masses refer to differently labeled and alkylated species (upper panel). Upon fragmentation, the one sulfur-labeled CSSH can distinguish whether the outer or the inner sulfur is labeled.*

4.2 Investigating the biological functions of LMW RSS in disulfide reductase-deficient mouse livers

We developed a robust experimental protocol to investigate sulfur metabolism *in vivo* in hepatocytes of mice lacking both vital reducing systems (full-body GR knockouts and hepatocyte-specific TrxR1 knockouts). In normal hepatocytes the main cellular source of CSH is the reduction of the disulfide bond in CSSC that was taken up via the xCT antiporter. Therefore, our collaborative research team has long been interested in how CSH homeostasis is maintained in TR/GR-null livers. The increased sensitivity to inhibition of the transsulfuration pathway suggested that it is somehow involved in maintaining their CSH demand. Initially, we thought that transsulfuration promoted the production of CSH from Met, however this is a slow process with a high energy requirement. Therefore, to gain a deeper understanding of how transsulfuration contributes to CSH homeostasis in TR/GR-null mouse livers, we performed comprehensive metabolomic and stable-isotope-labeled fluxomic analyses.

4.2.1 Sulfur-based metabolomic analyses on resting mouse livers reveal major differences between genotypes

Sulfur-based metabolomic analyses were conducted on WT and TR/GR-null livers of mice to compare the differences in CSH metabolism between these genotypes. Livers were harvested and frozen in liquid nitrogen; after cryohomogenization, the HPE-IAM based RSS detection protocol was performed as described in the Methods section. Analyses of baseline metabolites showed higher levels of CSSC, CSH, CSSH, and GSH, but less Cth (Figure 11) in TR/GR-null vs WT livers.

CSSC levels were elevated in TR/GR-null livers, as expected, since they cannot use any NADPH to reduce the disulfide bond. Based on this deficiency, we also expected reduced CSH and GSH levels, but surprisingly, we detected elevated levels of both analytes, suggesting another pathway that can support CSH demand in these mutant mouse livers.

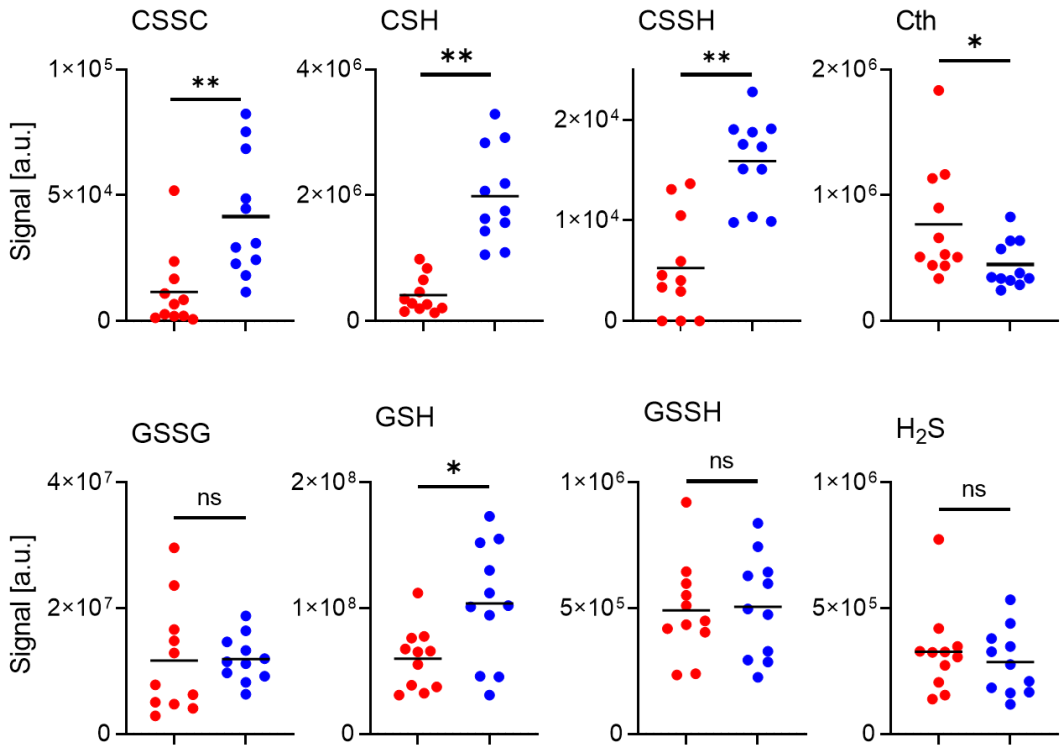

*Figure 11. **Metabolomic analyses of the RSS of a resting WT** (red) **or TR/GR-null** (blue) **mouse livers.** Perfused livers were harvested and cryohomogenized; thereafter, the HPE-IAM-based RSS detection protocol was performed for RSS metabolome analyses. Each data point represents an individual mouse, and the mean values are shown by the block lines. Differences in detected levels, based on a two-sided t-test, are not significant (ns; p>0.05), or significant with * p<0.05; ** p<0.01. (74)*

The transsulfuration pathway (as shown in Figure 2, green rectangle) can produce CSH from Met and Ser under CSSC-deprived conditions. A critical intermediate through this pathway is Cth. Therefore, the observed decreased level of Cth may suggest elevated transsulfuration activity in TR/GR-null mouse livers.

4.2.2 In TR/GR-null livers, canonical production of CSH via transsulfuration alone cannot sustain CSH homeostasis

To gain deeper insights into the mechanisms of CSH production via the transsulfuration pathway, stable-isotope-labeled fluxomic analyses were performed. Since only the sulur atoms traverse from Met to CSH, we applied sulfur-labeled Met ([^{34}S]-Met) to follow the sulfur throughout this pathway. Mice were inoculated with [^{34}S]-Met via a jugular catheter; this approach allows administration of a higher dose of labeled substrate for more efficient incorporation of isotope labeling into the metabolic fluxes of the livers. A

total amount of 4.8 mg from [^{34}S]-Met was inoculated over a 4-hour period. Mice were harvested, and livers were perfused with saline buffer, snap-frozen, and cryohomogenized, frozen metabolite extracts were sent to Prof. Gina deNicola's laboratory (Moffitt Cancer Center, Tampa, Florida, USA) for metabolomic analyses of the labeled and unlabeled analytes of the transsulfuration pathway.

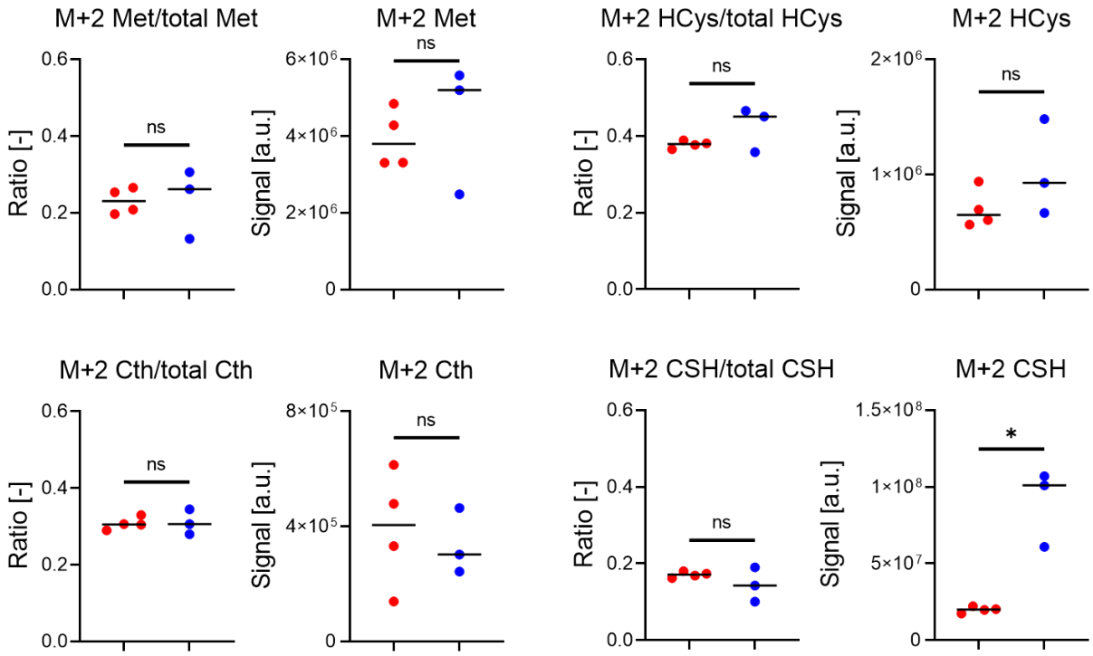

*Figure 12. **Mice with WT** (red) **or TR/GR-null** (blue) **liver were infused with [^{34}S]-Met** (4.8 mg over 4h), and the metabolites of the transsulfuration pathway were measured in Prof. Gina deNicola's Laboratory. Each data point represents an individual mouse (n=4 for WT and n=3 for TR/GR-null), and the mean values are shown by the block lines. Differences in detected levels, based on a two-sided t-test, are not significant (ns; p>0.05) or significant with * p<0.05. (74)*

We could not detect any differences in the labeled Met, Hcys, and Cth levels and ratios between the two genotypes (Figure 12), which indicated similar production and catabolic activities for these analytes. The only difference we detected was in the labeled level of M+2 CSH (Figure 12, lower right panels), which was elevated in mutant mouse livers, indicative of elevated transsulfuration activity; however, the labeling ratio didn't differ, suggesting that another Met-independent CSH-producing pathway should be upregulated.

4.2.3 TR/GR-null livers can obtain CSH from CSSC

After finding that the canonical Met-to-CSH transsulfuration pathway could not fully account for CSH production in mutant mice, we investigated the contribution of another

possible source of CSH, CSSC. Mice were infused with 4.8 mg [$^{13}C_6$,$^{15}N_2$]-CSSC over a 4-hour period. Followed by a similar protocol for metabolomic analyses as discussed previously in the Methods section.

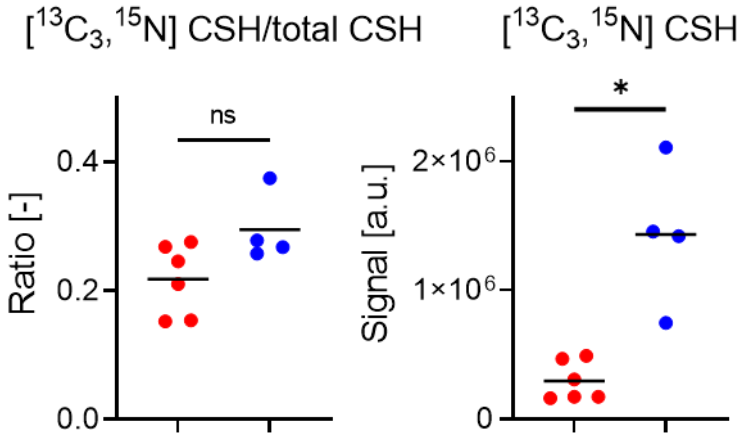

Figure 13. ***Levels and ratios of [$^{13}C_3$,^{15}N]-CSH generated in livers of [$^{13}C_6$,$^{15}N_2$]-CSSC-infused*** *(4.8 mg over 4h)* ***mice.*** *Each data point represents an individual mouse (n=6 for WT (red), n=4 for TR/GR-null (blue)), and the mean values are shown by the block lines. Differences in detected level, based on a two-sided t-test not significant (ns; p>0.05) or significant with * p<0.05. (74)*

An increased amount of labeled CSH was detected in mutant mouse livers (Figure 13. left panel), indicating that although TR/GR-null livers cannot reduce disulfide bonds, they still obtain a large portion of their CSH from CSSC. Redoxins, in particular TRP14, are not the only enzymes that can use CSSC as a substrate. The pyridoxal-5-phosphate-dependent (PLP) transsulfuration enzymes Cbs and Cse can also utilize CSSC via noncanonical reactions, as shown in Figure 2, reaction 4. In this reaction, the product is CSSH, which, in this experiment, is represented by the labeled [$^{13}C_3$, ^{15}N] CSSH. We therefore measured [$^{13}C_3$, ^{15}N] CSSH to investigate this possibility and found elevated levels and ratios of this analyte in mutant mice (Figure 14), indicating elevated activities in one or both of these Cbs and/or Cse catalyzed reactions.

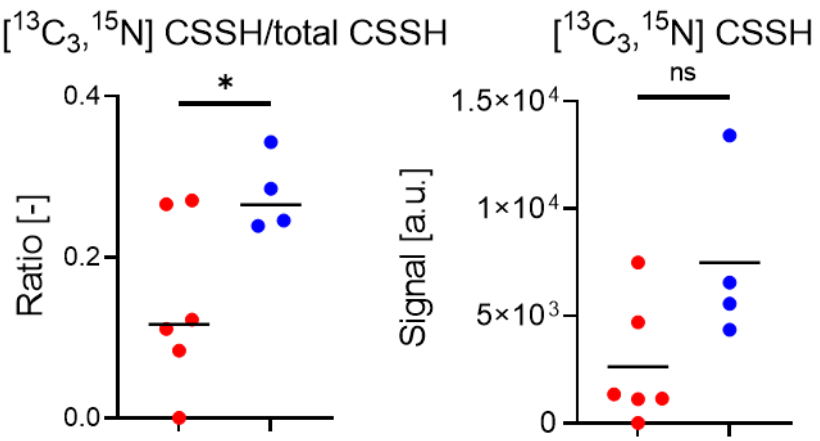

Figure 14. ***Levels and ratios of [$^{13}C_3$,^{15}N]-CSSH generated in livers of [$^{13}C_6$,$^{15}N_2$]-CSSC-infused*** *(4.8 mg over 4h)* ***mice.*** *Each data point represents an individual mouse (n=6 for WT (red), n=4 for TR/GR-null (blue)), and the mean values are shown by the block lines. Differences in detected level, based on a two-sided t-test, are not significant (ns; p>0.05) or significant with * p<0.05. (74)*

4.2.4 CSH production in TR/GR-null, but not in WT livers, is PLP-dependent

To further investigate the roles of Cbs and Cse in CSSH and CSH production, mice with WT or TR/GR-null livers were treated with their inhibitors before the labeled CSSC was administered. Aminooxoacetic acid (AOAA) blocks all PLP-dependent enzymes, including both Cbs and Cse. Treatment with this inhibitor significantly decreased the ratio of labeled CSSH, supporting that CSSH is a direct product of Cbs and Cse (Figure 2, reaction 4). This reaction represents the cleavage of the C-S bond in CSSC, resulting in labeled CSSH, which may be further transformed into CSH to support the CSH demand.

Both the amounts and the ratios of labeled CSH decreased in mutant mice, but not in the WT, upon AOAA treatment. This corroborates the hypothesis that TR/GR-null mice can gain CSH from CSSC through C-S bond cleavage by Cbs and/or Cse. In this multi-step reaction, the first product is the labeled CSSH.

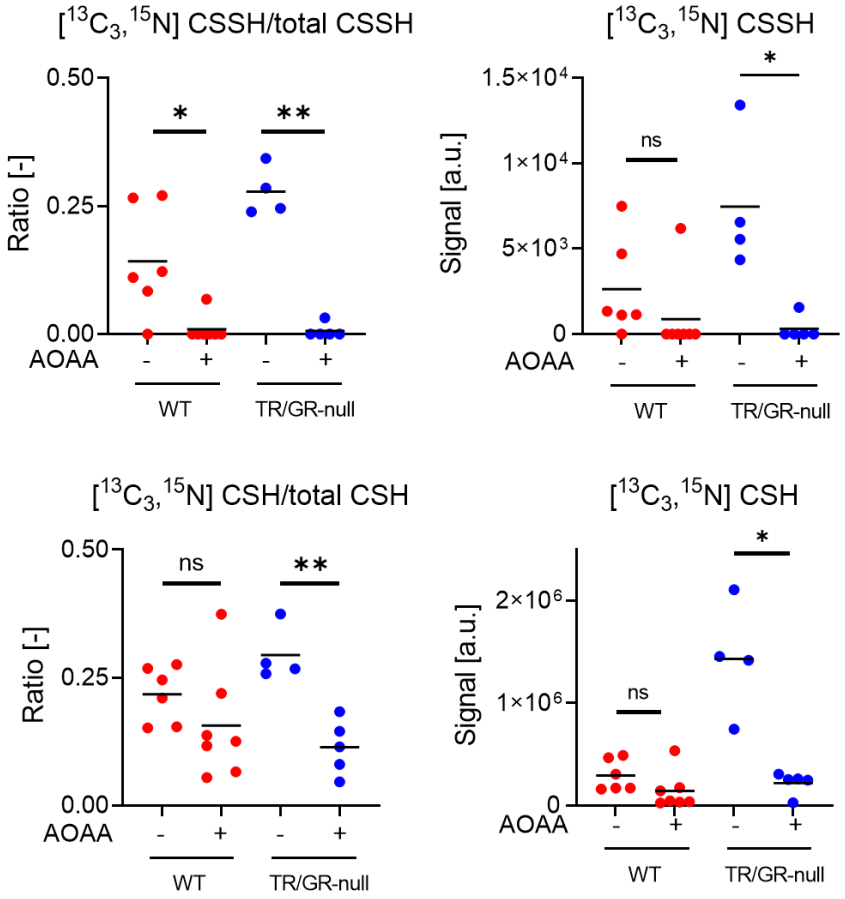

Figure 15. ***The amount and ratio of the [$^{13}C_3$,^{15}N]-CSH and [$^{13}C_3$,^{15}N]-CSSH from livers of [$^{13}C_6$,$^{15}N_2$]-CSSC- infused*** *(4.8 mg over 4h)* ***mice, with or without AOAA treatment.*** *(The untreated data is the same data set as shown in Figures 13. and 14.) Each data point represents an individual mouse (WT (red) n=6 for untreated and n=7 for AOAA treated, TR/GR-null (blue) n=4 for untreated and n=5 for AOAA treated), and the mean is shown. Differences in detected level, based on a two-sided t-test, are not significant (ns; p>0.05) or significant with * p<0.05. (74)*

4.2.5 CSSH is an intermediate in PLP-dependent CSH production

To further corroborate the proposed mechanism, we aimed to detect the first product of the CSSC-Cse or -Cbs reactions to be able to distinguish this reaction from other enzymatic reactions that can generate CSSH.

Infusing mice with sulfur-labeled [$^{34}S_2$]-CSSC, the first intermediate of these pathways should be [$^{34}S_2$]-CSSH, which is labeled on both sulfurs, while CSSH arising from other enzymatic or non-enzymatic reactions (e.g., transpersulfidation of CSH) will have only one labeled sulfur ([^{34}S]-CSSH). (Hereafter, the labeled [^{34}S] will be indicated as **S**, and the total mass change of the analytes will be indicated as M+2 or M+4, depending on the number of S, e.g., [$^{34}S_2$]-CSSH for M+4 C**SS**H.) In the following experiments, we aimed to follow the **S** incorporation from M+4 C**SS**C into M+2 C**S**H, as shown by the following reactions. As discussed before, the differentially labeled CSSH species can be identified using tandem mass spectrometry based on their different masses or fragmentation patterns (Figure 10), which can give deeper insight into the mechanism of these reactions.

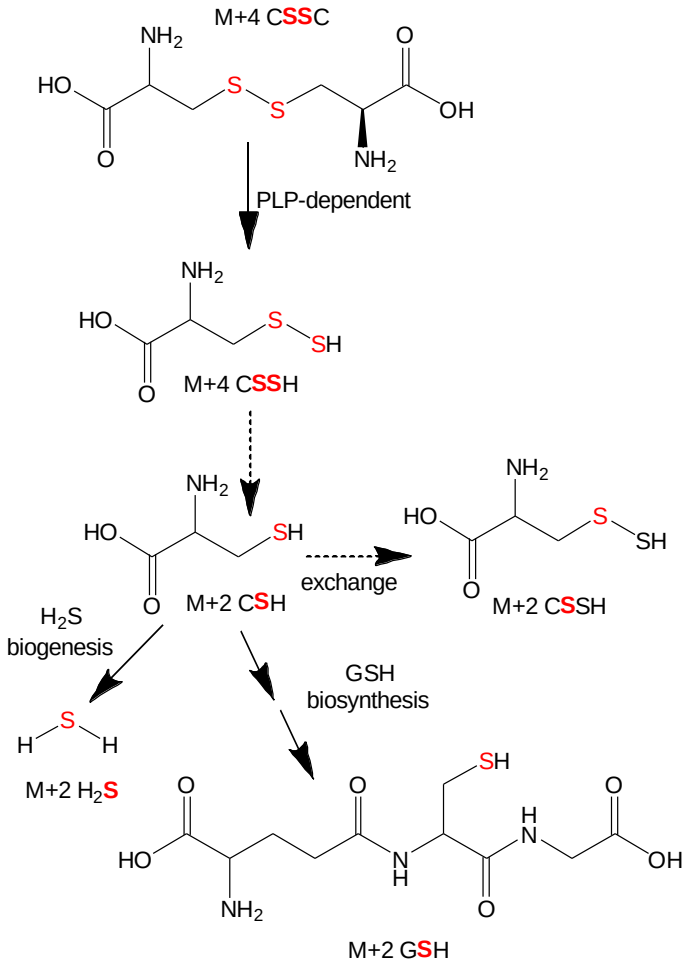

Figure 16. ***PLP-dependent possible utilization of CSSC in TR/GR-null livers for CSH and GSH biosynthesis.*** *Solid arrows illustrate enzymatic reactions, whereas dashed arrows represent non-enzymatic reactions. (74)*

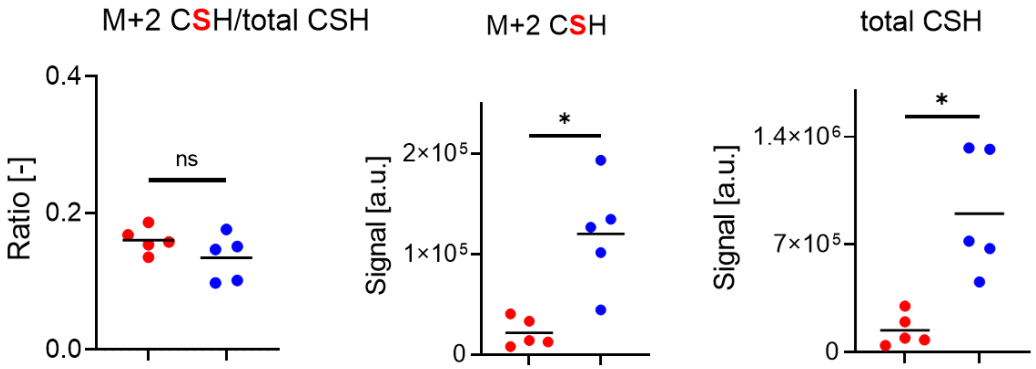

Figure 17. ***The amount and ratio of CSH and the total CSH from livers of CSSC-infused*** *(4.8 mg for 4 hours, WT (red) n=5, TR/GR-null (blue) n=5)* ***mice****. Each data point represents an individual mouse, and the mean values are shown by the block lines. Differences in detected level, based on a two-sided t-test, are not significant (ns; p>0.05) or significant with * p<0.05. (74)*

We detected greater enrichment of the labeled CSH in mutant mice, similar to that in the [$^{13}C_6$, $^{15}N_2$] CSSC infusion experiment (Figure 17. and 13, respectively).

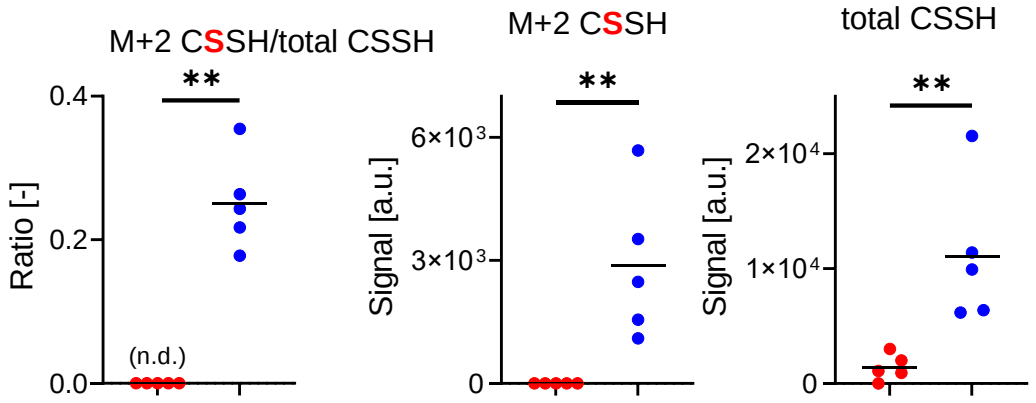

Figure 18. ***The amount and ratio of CSSH*** *(proximally labeled)* ***and the total CSSH from livers of CSSC-infused*** *(4.8 mg for 4 hours, WT (red) n=5, TR/GR-null (blue) n=5)* ***mice****. Each data point represents an individual mouse, and the mean values are shown by the block lines. Differences in detected level, based on a two-sided t-test, are not significant (ns; p>0.05) or significant with * p<0.05; ** p<0.01. (74)*

Labeled CSSH was only detected in mutant mice, and we observed only proximal M+2 CSSH labeling, as shown in Figure 18. This species can be generated through a labeled M+2 CSH, gaining an unlabeled S, suggesting that labeled M+2 CSH must be generated as a precursor of this molecule. Unfortunately, we weren't able to detect M+4 CSSH, the

first intermediate in the Cbs/Cse catalyzed CSSC utilization process. We suspect that the turnover of this species to form CSH should be too rapid for detection *in vivo*.

4.2.6 Isolated primary hepatocytes sustain their CSH levels

To verify production of the M+4 C**SS**H intermediate, we isolated primary hepatocytes, treated them with M+4 C**SS**C for the indicated time period, and monitored isotope flux in WT and TR/GR-null cells. The viability of the isolated hepatocytes was validated by detecting acidification of the media due to mitochondrial respiration, CSSC uptake, and its consequent metabolic products in the cells.

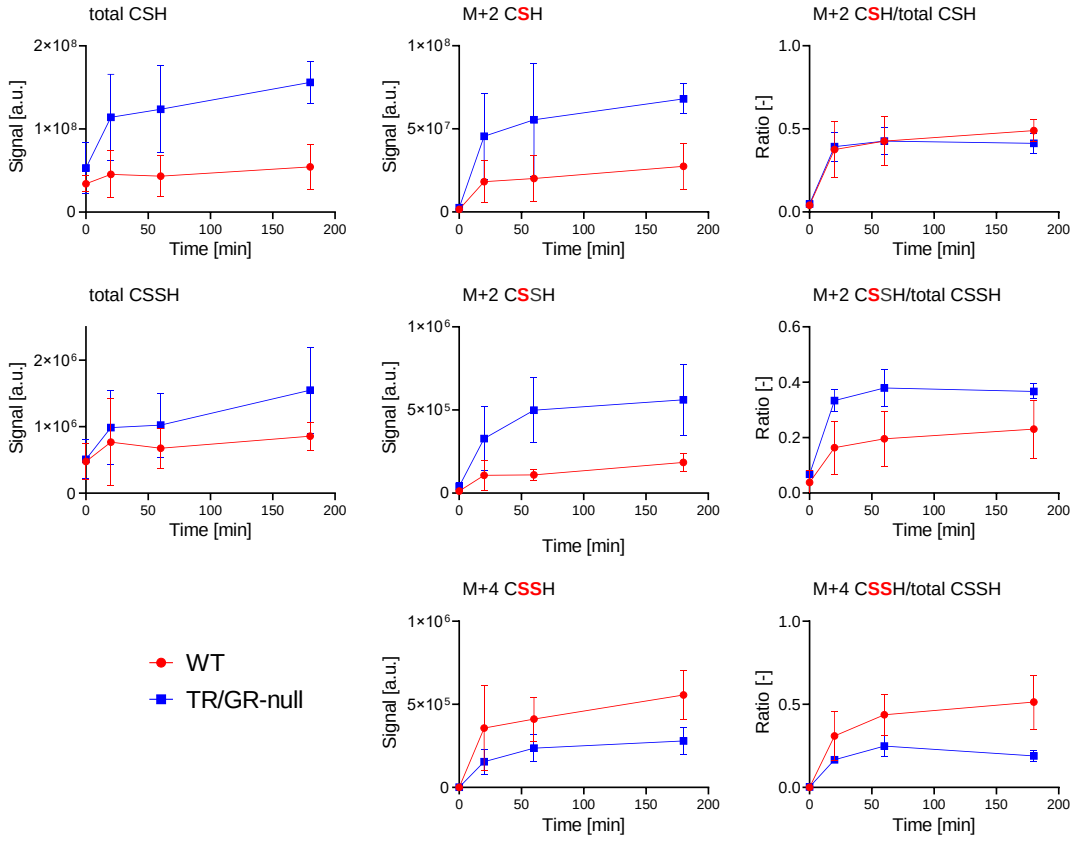

Figure 19. ***The ratio, the total and the labeled amount of the CSH and CSSH species in M+4 CSSC treated primary hepatocytes*** *(WT red, TR/GR-null blue). Each point represents the mean value derived from primary hepatocytes obtained from four distinct isolations (n=4 per genotype from separate mice). Error bars indicate SD. (74)*

Mutant cells had elevated levels of labeled and unlabeled CSH but exhibited similar fluxes of isotope labeling (Figure 19 upper panels), with the same pattern as in the *in vivo* experiments. Total CSSH was also elevated in mutant cells, investigating the isotope

partitioning in CSSH species showed that M+2 C**S**SH levels and ratio are higher in the TR/GR-null hepatocytes compared to the WT (Figure 19, middle panels). This same pattern was observed in the livers, too; the M+2 C**S**SH level and ratio were higher in the mutant mouse livers, but were not detected in WT livers.

In this cellular system, we were able to detect the short-lived intermediate, M+4 C**SS**H (Figure 19, lower panels). Interestingly, WT cells temporarily accumulated more from this persulfide species than TR/GR-null hepatocytes. We hypothesize that the reason behind this is the possibility that in TR/GR-null cells, the consumption of M+4 C**SS**H might be faster, because this is the only source of M+2 C**S**H. Note, that WT cells can use NADPH to reduce the CSSC disulfide bond; in TR/GR-null cells, they can only form M+2 C**S**H via M+4 C**SS**H. With this experiment, we also validated that CSH synthesis in both genotypes is cell autonomous and does not rely on other organs or other cell types.

4.2.7 CSH production in TR/GR-null hepatocytes is Cse-dependent

To distinguish which PLP-dependent enzymes participate in CSH production, we used the inhibitor propargyl glycine (PAG) because it specifically inhibits Cse but not Cbs, and performed stable-isotope tracing. The cells were pretreated with 1 mM PAG for 24 hours to block Cse prior to adding M+4 C**SS**C, which was added for 24 hours together with 1 mM inhibitor. The detected labeled and total CSH and CSSH levels are shown in Figure 20.

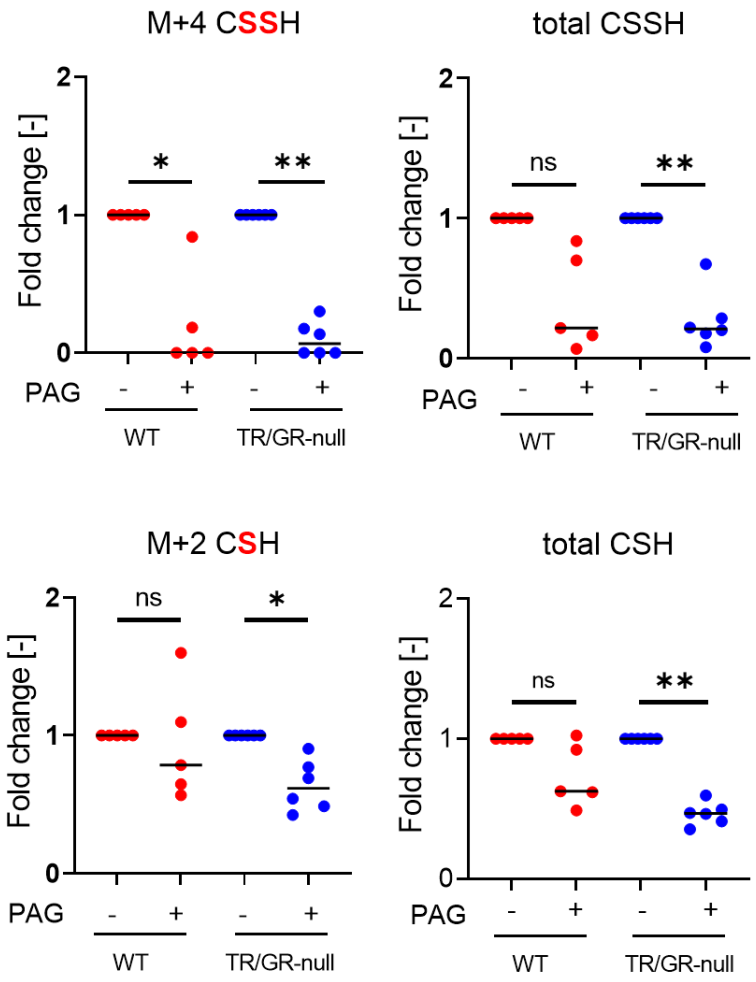

Figure 20. ***The amount of labeled CSH and CSSH and the total CSH, CSSH from M+4 CSSC-treated*** *(24 h, 200 µM)* ***primary hepatocytes with or without PAG treatment*** *(48h, 1 mM) (WT red, TR/GR-null blue), data are normalized to their untreated group within each genotype. Each data point represents a different isolation from an individual mouse (n=5 for WT and n=6 for TR/GR-null from separate mice), and the mean values are shown by the block lines. Differences in detected level, based on a two-sided t-test, are not significant (ns; p>0.05) or significant with * p<0.05; ** p<0.01. (74)*

We observed inhibitor-induced decreases in the M+4 CSSH in both genotypes (Figure 20 upper panels), confirming that this species is produced through Cse catalysis. The observed huge drop indicated that Cse plays a major role in M+4 CSSH production in both genotypes. Reduced levels of total and labeled CSH were detected in mutant but not in WT hepatocytes following PAG treatment (Figure 20 lower panels), suggesting that the primarily PLP-dependent CSH production in TR/GR-null hepatocytes is related to Cse.

4.2.8 Production of CSH in different genotypes depends on different cofactors

We performed *in vitro* experiments using freshly prepared liver lysates to test the effects of different cofactors on CSH production from CSSC. M+4 CSSC was added to the liver lysates together with PLP and/or NADPH, and to further verify Cse contributions, PAG was used in the indicated samples. Levels of M+4 CSSH, pyruvate, and M+2 CSH were monitored, where M+4 CSSH and pyruvate are the two products of the Cse-mediated CSSC C-S bond cleaving reaction (Figure 16). As expected, M+4 CSSH and pyruvate (shown in Figure 21) production was significant only in the presence of PLP and the absence of PAG, which further supported that CSSH production is indeed Cse-dependent in both genotypes.

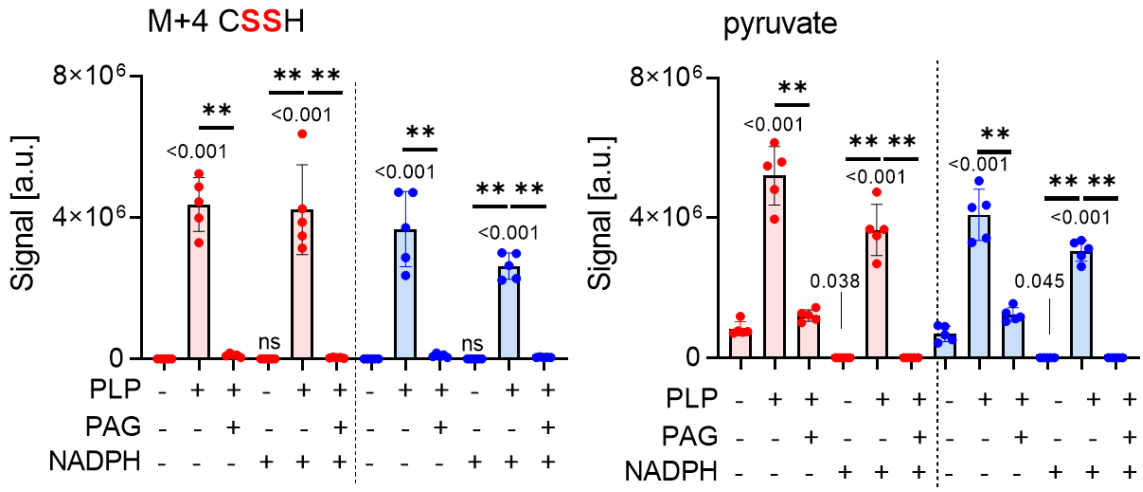

Figure 21. ***The amount of M+4 CSSH and pyruvate generated by liver lysates based on different cofactors*** *(WT red, TR/GR-null blue). All graphs show lysates from 5 different mice. Lysates were incubated with CSSC and PLP and/or NADPH for 30 min at 25°C, where indicated. Inhibitor (PAG) was added before initiating the reaction. P values are indicated above the column, compared to the left (no cofactors or inhibitors) of that genotype. ** represents p<0.01 between the compared groups. One-way ANOVA was used. (74)*

We detected a significant amount of M+2 CSH, but the WT and mutant lysates showed distinct patterns (Figure 22). In the WT, adding PLP and/or NADPH resulted in significant M+2 CSH production, whereas PAG treatment decreased it when only PLP was present. Adding NADPH produced much more M+2 CSH than PLP alone. Notwithstanding, TR/GR-null lysates could not use NADPH to reduce the disulfide bond in CSSC; only PLP-dependent C-S bond cleavage could produce CSH, which was inhibited by PAG.

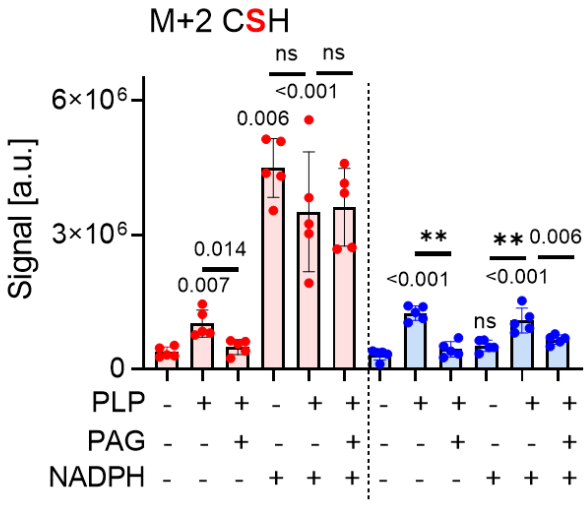

Figure 22. ***The amount of CSH generated by liver lysates based on different cofactors*** *(WT red, TR/GR-null blue). All graphs show lysates from 5 different mice. Lysates were incubated with CSSC and PLP and/or NADPH for 30 min at 25°C, where indicated. Inhibitor (PAG) was added before initiating the reaction. P values are indicated above the column, compared to the left (no cofactors or inhibitors) of that genotype. Ns p>0.05; ** represents p<0.01 between the compared groups. One-way ANOVA was used. (74)*

Although the NADPH-dependent reaction was more effective in producing M+2 CSH from M+4 CSSC in WT lysates, these experiments confirmed that in TR/GR-null livers, Cse-mediated C-S bond cleavage can produce substantial amounts of M+2 CSH from M+4 CSSC. Therefore, we propose that in the absence of disulfide reductases, this pathway can become the main source of CSH.

4.2.9 CSSH decomposition is a non-enzymatic reaction

We expressed and purified recombinant Cse to conduct enzyme kinetic experiments on the reactions in Figure 23. Cse was incubated with only its cofactor (PLP) in the presence of [$^{13}C_6$,$^{15}N_2$]-CSSC, and the analytes below were monitored.

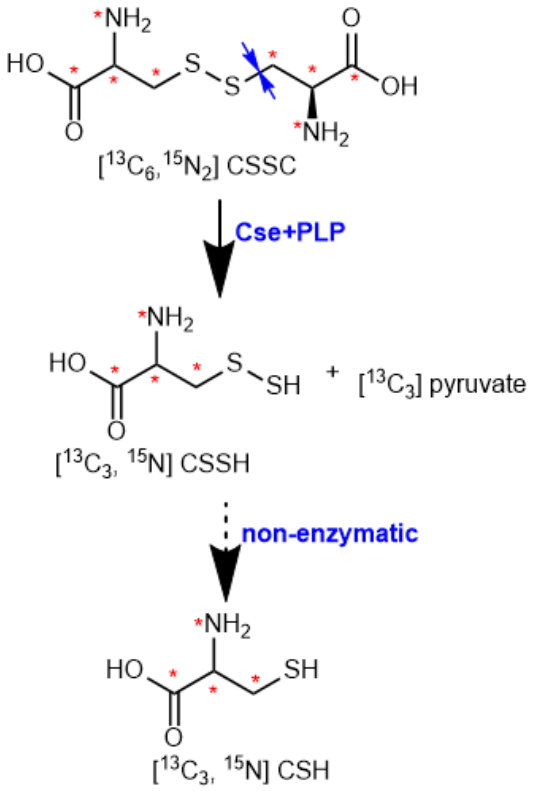

Figure 23. ***The proposed Cse-mediated C-S bond cleavage-based CSH-producing pathway****. Red star marks stable isotope-labeled atoms. Solid arrows illustrate enzymatic reactions, whereas dashed arrows represent non-enzymatic reactions. (74)*

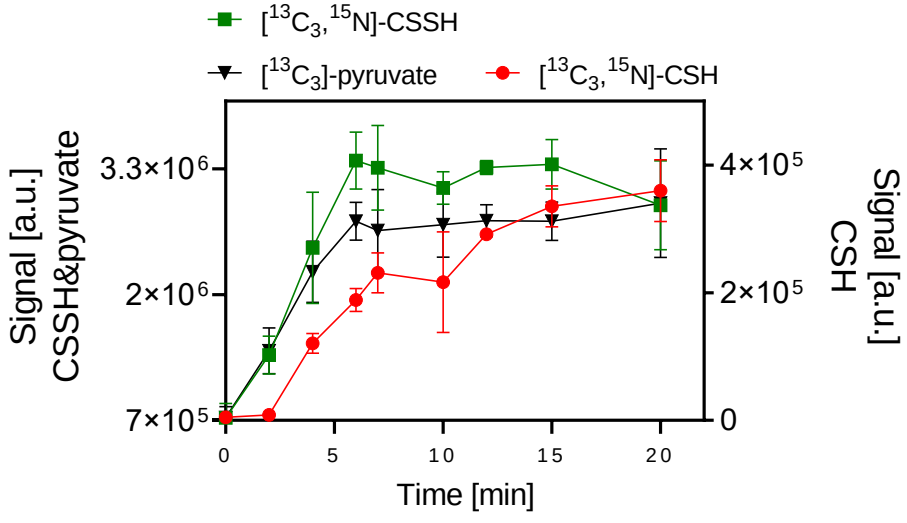

Figure 24. ***The amount of [$^{13}C_3$,^{15}N]-CSSH, [$^{13}C_3$]-pyruvate, and [$^{13}C_3$,^{15}N]-CSH generated by recombinant Cse in an in vitro reaction.*** *Recombinant Cse was incubated at 25°C with [$^{13}C_6$,$^{15}N_2$]-CSSC for the indicated times. The specified analytes were measured by HPLC-MS/MS, CSSH, and CSH were alkylated. (74)*

Time-resolved changes in the levels of the monitored analytes can be seen in Figure 24. The production of [$^{13}C_3$,^{15}N]-CSSH and [$^{13}C_3$]-pyruvate was rapid; it began to increase immediately upon the addition of the substrate and cofactor. However, a slight delay is observed in the production of the labeled CSH. This suggested that the first reaction in this system is Cse-mediated and very fast, while the second, CSH formation step, is a non-enzymatic reaction, which requires prerequisit formation of CSSH.

4.2.10 PAG treatment diminishes CSH levels in TR/GR-null mice

To validate the role of Cse in CSH production *in vivo*, TR/GR-null mice were treated with PAG and metabolomic analyses were carried out.

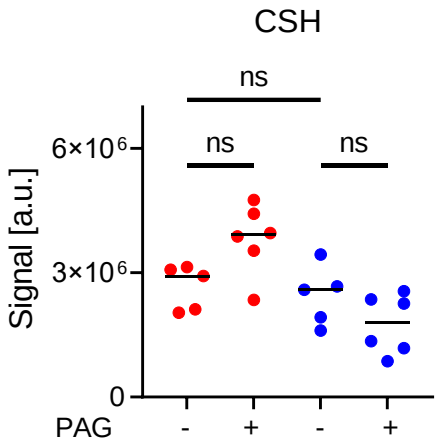

Figure 25. ***Impact of PAG treatment in WT*** *(red)* ***and TR/GR-null*** *(blue)* ***on plasma CSH levels****. Mice were administered intraperitoneal injections every hour for a duration of four hours with 10 mg/kg of PAG or saline, as specified, and were subsequently euthanized at the fifth hour. HPE-IAM-based detection was performed. n=5 for untreated in both genotypes; n=6 in each genotype for PAG-treated. The mean values are shown by the block lines. Differences in detected levels are not significant (ns; p>0.05). (74)*

In the plasma from the mice (Figure 25); no decrease in CSH levels was observed for either genotype. However, in the livers (Figure 26), CSH level decreased in the mutant after PAG treatment, but not in the WT. This correlates with our previous findings that CSH production is Cse-dependent in the mutant but not in WT livers, and that the liver CSH pool is organ-specific and is not influenced by circulating CSH produced by other organs.

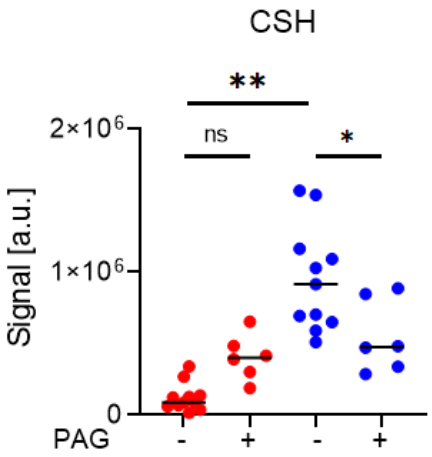

Figure 26. ***Impact of PAG treatment on WT*** *(red)* ***and TR/GR-null*** *(blue)* ***liver CSH levels****. Mice were administered intraperitoneal injections every hour for a duration of four hours with 10 mg/kg of PAG or saline, as specified, and were subsequently euthanized at the fifth hour. HPE-IAM-based detection was performed. Each data point represents an individual mouse (n=11 for untreated genotypes and n=6 for PAG treated genotypes). The mean values are shown by the block lines. Differences in detected levels are not significant (ns; p>0.05) or significant with * p<0.05; ** p<0.01. (74)*

4.3 Measurements of protein persulfide levels in PDAC metastasis formation

My endeavor was to measure HMW RSS, specifically protein persulfides (P-SSH). Although the analysis of protein persulfides often requires specialized proteomic platforms and sample preparation. However, after digesting the samples with pronase, our LMW persulfide detection protocol was suitable for analysis. Unlike most other digestive enzymes used in proteomics, which cleave between specific amino acids, pronase cleaves between each amino acid, yielding free, individual amino acids while keeping the S-S bonds intact. Hence, the digested free CSH and CSSH can be analyzed by our optimized HPLC-MS/MS method provide information about the overall protein-persulfidation.

In our previous study, we investigated how Cbs contributes to the metastatic transition of pancreatic ductal adenocarcinoma (PDAC) (12). We found that Cbs plays an important role in PDAC cells in the epithelial-to-mesenchymal transformation (EMT) through the Wnt signaling pathway. To establish this, I utilized this method to measure total protein persulfide levels in control and Cbs-knockdown PDAC cells. I found that Cbs silencing resulted in a drop in protein persulfide levels down to the levels found in non-metastatic PDAC cells values (Figure 27).

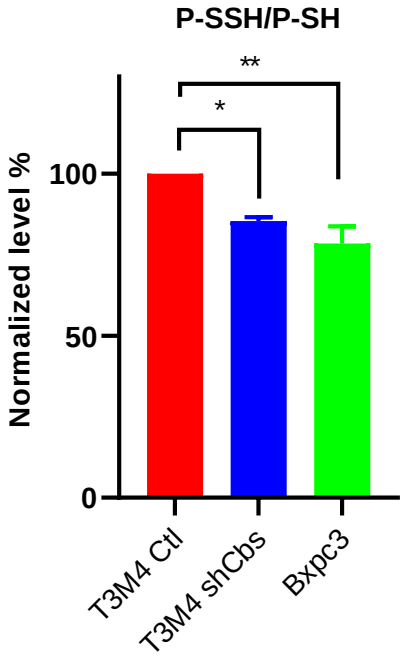

Figure 27. ***Protein persulfide ratio in T3M4 control and Cbs silenced, and in BxPc cell lines. (12)*** *The indicated cell lines were plated onto 12-well plates, and the next day, an HPLC-MS/MS-based protein persulfide measuring protocol was performed as described in 3.7. section. The data are normalized to the T3M4 control cell line. Differences in detected levels are not significant (ns; p>0.05) or significant with * p<0.05; ** p<0.01. (12) Abbreviations: P-SSH: protein persulfide, P-SH: protein thiol*

Later, our research group confirmed that this process was important in the deactivation of the STAT3 transcription factors in relation to EMT. Persulfidation can shield proteins from overoxidation and oxidative stress, thereby enabling thiol recovery even after overoxidation. The persulfidated STAT3 cannot form a dimer, which is its inactive form; hence, that pathway could stay active and drive cell proliferation and metastasis.

5 Discussion

The HPE-IAM-based LMW and HMW persulfide detection protocol, established by Akaike et al. (24), has become widely used for detecting RSS; however, the critical steps in sample preparation have not been well studied. Moreover, some alkylation parameters differ across studies without any explanation (from 20 min to 60 min (28, 70, 78)). For this reason, we reinvestigated critical steps of the LMW sample preparation protocol and the experimental setup of the HPLC-MS/MS method.

We found that cell confluency, an often-overlooked parameter, can critically influence measurement outcomes. Cbs and Cse activites were highly influenced by cell density. Both enzymes promote cell proliferation (11, 12) and under overly confluent conditions, their expression diminishes, which likely accounts for the decreased persulfide levels we measured in overly confluent cultures (Figure 4). To investigate the RSS producing functions of these enzymes or the dynamics of the cellular RSS pool, it is important to maintain consistent cell confluency throughout their studies, ideally around 80-90% ($4x10^5$ cell/ml).

We found that lower temperatures during sample preparation, including cell lysis, are favorable for protecting persulfide species from degradation. Furthermore, scraping the cells on ice preserves LMW persulfide levels. Alkylation parameters have a significant effect on the speciation of the detected RSS species; therefore, these parameters also need to be tightly controlled. Data in Figure 6 suggest that higher temperatures (45°C) likely degrade persulfide species, causing them to be falsely detected as thiols. Alkylation at a lower temperature (37°C) is slower but better preserves CSSH species. Our temperature/time optimization indicated that at 37°C with HPE-AIM, 20 min is enough to reach complete derivatization. Longer times, however, increase the detected amount of H_2S; saturation isn't reached after 60 min. As our group published before, the detection of H_2S with derivatization utilizing a protocol (77) is problematic due to the liberation of H_2S from biological sulfide reserves. It requires strict timing for the alkylation and, because the HPE-IAM based protocol also gives information on H_2S levels, we emphasize that precise timing of the alkylation step is a critical requirement for reproducible results. We propose that 20 min at 37°C achieves representative alkylation of thiols, persulfides, and H_2S, so we have used these parameters as our standard protocol

across experiments. It is also noteworthy that extended alkylation times allow alkylation of not only thiol species but also amino groups, a frequent side reaction when using iodoacetamide derivatives (79). The alkylation time can be tightly controlled by effective quenching by acidification and keeping the samples at 4°C. Our data revealed that alkylation is ineffective at 4°C; hence, storing the samples on ice between each step will ensure that unwanted reactions (alkylation) during sample preparation will not occur. Moreover, temperature control of the HPLC autosampler at 4°C ensures sample stability prior to injection. Nevertheless, prompt measurement of the samples is favored to avoid RSS degradation. To address this, we optimized our HPLC-MS/MS method to reduce the time samples spend in the autosampler.

The optimized method enables us to measure LMW and HMW persulfides in various biological samples and obtain reliable data. Mass spectrometric detection also enables us to use stable-isotope-labeled amino acids and perform time-resolved fluxomic analyses to investigate the contributions of different metabolic pathways.

We used the optimized HPE-IAM based method and integrated fluxomic analyses in several studies: for example, this method revealed that, under TRP14 deficiency, the transsulfuration pathway becomes more active to support the CSH demand (22).

We performed steady-state metabolomic analyses on disulfide reductase-deficient mouse livers and found elevated levels of CSSC, CSH, GSH, and even CSSH. These data suggested that the existence of alternative efficient CSH-producing pathway(s) exists in these mutant livers. To uncover the origin of the CSH, we had to develop an *in vivo* model system that allows us to monitor sulfur metabolism.

Performing stable isotope tracing in *in vivo* studies is complex, and the method of administering the isotopically labeled amino acids is crucial. While in *in vitro* studies, administering the isotopically labeled amino acids can be as simple as adding to or changing the media, in *in vivo* studies it is not so straightforward. To obtain reliable and reproducible results, our group established a protocol, where the isotopically labeled amino acid was administered via a jugular catheter, enabling a continuous infusion rather than a single high-dose administration. Jugular catheterization coupled with our HPLC-MS/MS method indeed provided a robust, reliable platform for investigating the *in vivo* metabolic pathways of RSS.

Administration of [^{34}S]-labeled Methionine allowed us to follow the labeled sulfur through the transsulfuration pathway in both genotypes. We found that, although the canonical CSH producing activity is slightly elevated, this pathway cannot fully account for CSH production in TR/GR-null mouse livers.

Using [$^{13}C_6$,$^{15}N_2$]-CSSC, we revealed that, despite TR/GR-null mice being unable to reduce the S-S bond in CSSC, they can still obtain CSH from CSSC. Importantly, the redoxins, particularly TRP14, as well as other thioredoxins and glutaredoxins, are not the only enzymes that can use CSSC as a substrate. Based on Figure 2, Cbs and Cse can also use CSSC as a substrate to produce CSSH; accordingly, we detected an elevated level of labeled CSSH in the TR/GR-null mouse livers compared to WT. These reactions are PLP-dependent, so we used AOAA to inhibit PLP-dependent enzymes and investigate their significance.

AOAA was either administered to mice for steady-state metabolomics or used in tracing studies. Resting metabolomic analyses revealed that CSSH levels decreased in response to AOAA treatment in both genotypes, whereas CSH levels decreased only in the mutants (74). These findings were confirmed using labeled [$^{13}C_6$,$^{15}N_2$]-CSSC with AOAA. The inhibitor treatment caused a significant decrease in the ratio and labeled levels of CSSH in both genotypes; however, labeled CSH and its ratio decreased only in TR/GR-null livers. These experiments confirmed that CSH production in TR/GR-null but not in WT mice is PLP-dependent.

To get deeper insights into which metabolic pathways are responsible for this effect, we conducted a more comprehensive evaluation of the CSSC-CSSH reaction, using [$^{34}S_2$]-CSSC (M+4 C**SS**C). The major aim of this experiment was to capture the double-labeled M+4 C**SS**H species, which should be the first intermediate in the enzymatic reaction when CSSC is used as a substrate for Cse and Cbs. Mice were infused with M+4 C**SS**C, and thiol and persulfide species were monitored. The mutant mice had higher CSH levels than WT mice, which correlates with our previous results. Examining the CSSH persulfides, we were able to detect only one-sulfur-labeled M+2 C**S**SH, and this was detected only in the mutant livers; M+4 C**SS**H wasn't detectable in the livers of either genotype. But the M+2 C**S**SH, where the inner sulfur is labeled, suggested that the labeled M+2 C**S**H must be formed in the first step, and the persulfidation occurs afterward. M+4 C**SS**H is a highly

reactive and labile intermediate; we concluded that this was due to the fast decomposition in an *in vivo* environment.

We examined different *in vitro* systems to validate the CSSC-CSSH-CSH reactions. First, primary hepatocytes were isolated from both genotypes, and fluxomic analyses were performed using M+4 C**SS**C. Isolated TR/GR-null hepatocytes were viable and metabolically active; they obtained more M+2 C**S**H from M+4 C**SS**C than did the WT hepatocytes. In this system, we were able to measure M+2 C**S**SH and M+4 C**SS**H. The M+2 C**S**SH showed the same pattern as *in vivo* studies: elevated enrichment in TR/GR-null cells. Interestingly, M+4 C**SS**H levels were lower in mutant cells than in WT cells; we suggest this may be due to increased turnover in mutant cells.

We were able to capture this labile species in isolated hepatocytes; moreover, we applied a specific inhibitor to further investigate the roles of Cbs and Cse in CSH production in TR/GR-null cells. At first, we used AOAA as a semi-selective inhibitor of PLP-dependent enzymes, but in hepatocytes, we further narrowed it to a Cse-selective inhibitor, PAG. Isotopic labeling with inhibitor treatment confirmed that Cse is the main enzyme in M+4 C**SS**H production from M+4 C**SS**C in both genotypes. In the labeled M+2 C**S**H, the PAG treatment resulted in a significant decrease in mutant cells but not in WT cells. These results confirmed that CSH production in the TR/GR-null genotype is Cse-mediated, via CSSH as an intermediate.

TR and GR use NADPH as a source of electrons; Cse and Cbs need PLP as a cofactor for their activities. Therefore, we performed an *in vitro* experiment to test the cofactor dependency of CSH production in the genotypes. We used liver lysates and added M+4 C**SS**C to induce the enzymatic reactions. M+4 C**SS**H and pyruvate were produced only in the reaction mixtures with PLP, and PAG treatment inhibited their production. This confirmed that the C-S bond cleavage in CSSC is Cse-mediated. Accumulation of these two analytes did not differ much across genotypes. However, in CSH, a different pattern emerged. In WT livers, NADPH-dependent reactions were the main CSH producing pathways, whereas in the TR/GR-null lysates, CSH was produced only when PLP was added. This experiment corroborates our prediction that CSH production in WT is NADPH- and disulfide-bond-reduction-dependent, whereas in TR/GR-null livers it is PLP-dependent and occurs via C-S bond cleavage. These data also indicate that NADPH-

dependent CSH formation is the more efficient pathway; but, in primary hepatocytes and *in vivo*, C-S bond cleavage reaction is the sole mechanism for CSH production in TR/GR-null hepatocytes.

Reaction 1 (WT): $CSSC \xrightarrow{Trp14,\ TR,\ NADPH} 2\ CSH$

Reaction 2 (TR/GR-null): $CSSC \xrightarrow{Cse,PLP} CSSH \rightarrow\rightarrow CSH$

This experiment also suggested that the formation of CSH from CSSH is not an enzymatic reaction, as no other cofactors were needed for the conversion of CSSH to CSH. We tested this prediction using recombinant Cse, where only the enzyme, PLP, and [$^{13}C_6$,$^{15}N_2$]-CSSC were present. [$^{13}C_3$,^{15}N]-CSSH and [$^{13}C_3$]-pyruvate levels started to increase immediately after the addition of the cofactor and the substrate, while the appearance of [$^{13}C_3$,^{15}N]-CSH was delayed. These data confirmed two major points: i) CSSH is a precursor of CSH, and ii) the transformation from CSSH into CSH is not an enzymatic reaction.

We validated the above-described *in vitro* findings in mice. Administering PAG to resting animals confirmed that CSSH levels in the liver were Cse-dependent, because they decreased in both genotypes following PAG treatment; however, as expected, CSH levels decreased only in TR/GR-null livers. We examined the plasma of these animals and found that the inhibitor treatment did not alter plasma CSH levels in either genotype, confirming that CSH production is cell autonomous in liver and that the CSH demand in TR/GR-null cells is not met by CSH generated in other organs.

The Cse C-S bond-cleaving reaction had been described earlier (25). Those authors suggested that Cse can generate CSSH from CSSC more effectively than Cbs, but they didn't investigate CSH formation afterward. Moreover, the *in vivo* importance of this reaction was called into doubt (25). Here, we demonstrated the significance of this reaction in a mouse model and confirmed that it can support the CSH demand in hepatocytes under disulfide reductase deficiency. Without isotope tracing, the importance of this pathway could not have been delineated, further strengthening the biological importance of robust RSS measurement technologies.

In another study, we showed that BRAF V600E inhibition therapy in melanoma induces Cse upregulation. Parallel metabolic reprogramming together allows this upregulated Cse to use CSSC as its primary substrate to produce elevated levels of CSSH, which is utilized by the cells to develop resistance to BRAF V600E targeted therapy (10). Due to treatment in melanoma cells, not only LMW but also protein persulfide species were elevated. For the examination of HMW persulfides, the same HPLC-MS/MS method for free amino acids that we use for LMW metabolites can be applied directly after total protein digestion with pronase. Using this approach, we investigated the roles of protein persulfides in different cancer model systems. In metastatic PDAC cells, Cbs showed a high expression, especially in T3M4 cells. Silencing Cbs (shCbs) in this cell line hindered metastasis formation in our mouse models; however, it did not alter the tumor size. Further investigation revealed that the STAT3 transcription factor is highly active in these cells and promotes epithelial-to-mesenchymal transition via Wnt signaling, a key step in metastasis. STAT3 can be persulfidated and protected from overoxidation-induced transcriptional activity loss. In the shCbs T3M4 cell line, decreased protein persulfide levels and increased STAT3-dimer were observed. This suggeted that Cbs contributes to STAT3 persulfidation in these cells and protects it from oxidation-induced damage. These data suggest that, if an effective drug targeting Cbs can be developed, it might serve as a therapeutic target in PDAC, leading to a less aggressive tumor phenotype and fewer metastases (12).

Both LMW and HMW RSS have important biological roles and functions. In this thesis, I critically re-evaluated and improved RSS detection methods, which enabled us to effectively investigate their functions and metabolic pathways in both cellular systems and whole-animal models.

6 Conclusions

This dissertation was focused on setting up robust and reliable RSS detection methods, which can give mechanistic insights into the biological actions of these reactive species.

Both quantitative and qualitative analyses of RSS are challenging due to their labile nature and high reactivity. To accurately and effectively measure them, a detailed and critical re-investigation of the applied protocols was needed. We demonstrated that **to preserve persulfide species, lower temperatures are required throughout the entire sample preparation process**, from cell scraping until injection in the autosampler. **Tight control of alkylating parameters** (temperature and time) **is required to obtain reproducible results**. However, to obtain reliable data, it was not enough to tightly control the alkylation protocol; it was also necessary to minimize artifact alkylation between the different steps. This could be achieved by keeping the samples on ice or by acidification. We successfully reduced the analysis time by 50%, thereby managed to shorten the time the samples are retained in the autosampler. The method was successfully used to measure RSS across various biological systems, including cultured cells, plasma, and tissue samples.

We further refined the method to perform stable-isotope tracing studies for metabolic pathway analyses and to **distinguish between differently labeled CSSH species in both *in vitro* and *in vivo* systems**.

We managed to identify **a previously overlooked adaptive sulfur metabolic pathway that maintains cysteine (CSH) production** when the major disulfide reductase systems, thioredoxin reductase (TR) and glutathione reductase (GR), are hindered. Using steady-state RSS-focused metabolomic analyses and *in vivo* isotope tracing, we showed that TR/GR-null mouse livers preserve CSH homeostasis **through a pyridoxal 5'-phosphate (PLP)-dependent, Cse-mediated mechanism that cleaves a C–S bond in CSSC as a first step**.

In TR/GR-null mouse models, we performed sulfur-based metabolomic analyses, which revealed increased levels of LMW thiol and persulfide species. Using carbon and nitrogen-labeled [$^{13}C_6$,$^{15}N_2$]-CSSC, we demonstrated that mutant mice, **although they are unable to reduce the disulfide bond in CSSC through NADPH-dependent reduction,**

can still obtain labeled CSH from CSSC. This result led to the identification of an alternative reaction in which PLP-dependent transsulfuration enzymes use CSSC as a substrate to generate CSSH, which can be further converted to CSH.

To further validate the role of Cbs and Cse in CSH production, we conducted **inhibitor studies** using AOAA and the Cse-specific inhibitor PAG. These experiments **corroborated that CSH production in TR/GR-null liver is** indeed **PLP-dependent and is predominantly mediated by Cse**. Although inhibition of PLP-dependent enzymes reduced CSSH levels in both genotypes, CSH levels decreased only in the mutant, thereby confirming that wild-type (WT) livers primarily rely on NADPH-dependent disulfide bond reduction, while TR/GR-null livers depend on Cse-mediated carbon-sulfur (C–S) bond cleaving reaction. Resting mice were treated with PAG, which further validated that the CSH homeostasis is Cse-dependent and cell-autonomous in the TR/GR-null mouse livers.

To gain mechanistic insight into this pathway, we applied [$^{34}S_2$]-CSSC and followed sulfur in *in vivo* and *in vitro* systems to determine how it is incorporated into thiol and persulfide species. Detection of selectively labeled persulfide species in mutant livers indicated that CSSH formation precedes CSH production and that CSSH is an extremely labile intermediate with rapid turnover *in vivo*. **In primary hepatocytes, our alkylation protocol was able to capture [$^{34}S_2$]-CSSH, thereby verifying the Cse-mediated CSH-producing pathway.** An elevated flux was found in the TR/GR-null hepatocytes in the labeled CSH and one-sulfur labeled CSSH. Although unexpectedly, levels of [$^{34}S_2$]-CSSH were lower in the mutant hepatocytes as compared to WT hepatocytes, we hypothesize that this could occur due to its higher turnover into other labeled species. Based on the high production of CSH from CSSH in these cells, we predict that this likely reflects accelerated turnover of CSSH to CSH.

In vitro liver lysate experiments and recombinant Cse assays conclusively demonstrated that: (i) CSSC C-S bond cleavage produces CSSH and pyruvate in a PLP-dependent reaction mediated by Cse; (ii) **CSH formation requires the prerequisition of CSSH**; and (iii) **the conversion of CSSH to CSH is a non-enzymatic process**. Importantly, NADPH-dependent CSH formation proved to be only prevalent in WT lysates, whereas

in TR/GR-null livers, the PLP-dependent pathway became the dominant and functionally sufficient route for maintaining CSH levels.

Collectively, our findings highlight the metabolic flexibility of sulfur metabolism. We demonstrate that under conditions of disulfide reductase deficiency, the liver activates a Cse-mediated, PLP-dependent C–S bond–cleaving pathway that bypasses the need for NADPH-dependent disulfide reduction. Although the conversion of CSSC into CSSH by Cse was previously described biochemically, it was considered biologically insignificant due to unfavorable substrate availability. Our isotope-tracing studies in TR/GR-null livers provided the first *in vivo* evidence of this reaction's biological relevance and adaptive importance.

Finally, we confirmed an important role for Cbs induced HMW persulfides in PDAC metastasis formation. We found that **Cbs plays a key role in persulfidating STAT3, thereby preventing dimerization-induced loss of activity**. Supporting this, in Cbs-silenced cell lines, a decrease in protein persulfidation and an increase in STAT3 dimer levels were observed. Additionally, in an orthotopic mouse model, fewer metastases were observed when Cbs-silenced cells were compared to control cells merely injected to induce tumor formation.

Our results demonstrated that LMW and HMW RSS play key roles in sulfur metabolism and redox homeostasis, and that the transsulfuration pathway is plastic and adaptive to support cell survival. With our optimized, stable-isotope tracing method, we can identify molecular mechanisms and gain deeper mechanistic insight into the metabolism of the RSS.

7 Summary

Intracellular redox balance is essential for cellular viability, proliferation, and regulating processes such as energy metabolism, signal transduction, and stress adaptation. An imbalance in redox homeostasis results in oxidative or reductive stress, which can lead to different diseases. Reactive Sulfur Species (RSS) are vital for maintaining intracellular redox balance, but their detection is challenging due to their high reactivity, which makes them labile. To enable biological studies of RSS, we first optimize and re-evaluate alkylating protocols that preserve their speciation and capture labile persulfide species. The optimized method thereby enabled us to investigate low- and high-molecular weight (LMW and HMW) persulfide species in various biological matrices and to gain deeper, mechanistic insight into their metabolism and biological roles.

The HPE-IAM-based LMW and HMW persulfide detection protocol is widely used due to HPE-IAM's stabilizing effect on these species. We critically re-evaluated this persulfide detection method to improve the reliability and reproducibility of our analyses. Using the improved method with stable isotope-labeled fluxomic analyses, we examined two complex biological systems: a disulfide reductase-deficient mouse model and a pancreatic ductal adenocarcinoma model. We showed that, under disulfide reductase deficiency, a PLP-dependent, Cse-mediated C–S bond-cleaving pathway can be activated, bypassing NADPH-dependent disulfide reduction of CSSC and thereby maintaining CSH homeostasis. Our *in vitro* and *in vivo* stable-isotope-tracing studies provided the first evidence that this pathway is indeed biologically relevant; moreover, it highlighted the metabolic flexibility of sulfur metabolism.

Additionally, we linked the transsulfuration enzyme Cbs to metastasis formation in PDAC tumors through HMW persulfides and demonstrated that posttranslational protein pesulfidation can affect protein activity, thereby initiating epithelial-to-mesenchymal transformation and metastasis formation.

The research outlined in this thesis expands our comprehension of the metabolic pathways of sulfur metabolites and the adaptability of these pathways. We gained a deeper mechanistic understanding of the roles of LMW and HMW persulfide species in sulfur metabolism and redox homeostasis.

8 References

1. Helmut Sies Ryan J. Mailloux, Ursula Jakob. Fundamentals of redox regulation in biology. Nat Rev Mol Cell Biol. 2024;25(9):701–19.

2. Celia María Curieses Andrés Fernando Lobo, José Manuel Pérez de la Lastra, Elena Bustamante Munguira, Celia Andrés Juan, Eduardo Pérez Lebeña. Reactive Sulfur Species and Protein Persulfidation: An Emerging Redox Axis in Human Health and Disease. Current Issues in Molecular Biology. 2025;47(9).

3. Zsolt Combi László Potor, Péter Nagy, Katalin Éva Sikura, Tamás Ditrói, Eszter Petra Jurányi, Klaudia Galambos, Tamás Szerafin, Péter Gergely, Matthew Whiteman, Roberta Torregrossa, Yuchao Ding, Lívia Beke, Zoltán Hendrik, Gábor Méhes, György Balla, József Balla. Hydrogen sulfide as an anti-calcification stratagem in human aortic valve: Altered biogenesis and mitochondrial metabolism of H(2)S lead to H(2)S deficiency in calcific aortic valve disease. Redox Biol. 2023;60:102629.

4. Constantin Munteanu Cristina Popescu, Andreea-Iulia Vlădulescu-Trandafir, Gelu Onose. Signaling Paradigms of H(2)S-Induced Vasodilation: A Comprehensive Review. Antioxidants (Basel). 2024;13(10).

5. Daniel Giovinazzo Biljana Bursac, Juan I Sbodio, Sumedha Nalluru, Thibaut Vignane, Adele M Snowman, Lauren M Albacarys, Thomas W Sedlak, Roberta Torregrossa, Matthew Whiteman, Milos R Filipovic, Solomon H Snyder, Bindu D Paul Hydrogen sulfide is neuroprotective in Alzheimer's disease by sulfhydrating GSK3beta and inhibiting Tau hyperphosphorylation. Proc Natl Acad Sci U S A. 2021;118(4).

6. Paul Bindu D, Pieper Andrew A. Protective Roles of Hydrogen Sulfide in Alzheimer's Disease and Traumatic Brain Injury. Antioxidants (Basel). 2023;12(5).

7. Suwarna Chakraborty Sunil Jamuna Tripathi, Edwin Vázquez-Rosa, Kalyani Chaubey , Hisashi Fujioka, Emiko Miller, Richa Tyagi, Thibaut Vignane, Sudarshana M. Sharma, Bobby Thomas , Zachary M. Weil, Randy J. Nelson , Milos R. Filipovic, Benjamin C. Orsburn , Solomon H. Snyder, Andrew A. Pieper, Bindu D. Paul Cystathionine γ-lyase is a major regulator of cognitive function through neurotrophin signaling and neurogenesis. Proceedings of the National Academy of Sciences of the United States of America. 2025;122(52).

8. Lital Argaev-Frenkel Tovit Rosenzweig. Redox Balance in Type 2 Diabetes: Therapeutic Potential and the Challenge of Antioxidant-Based Therapy. Antioxidants (Basel). 2023;12(5).

9. Rong-Hsuan Wang Pin-Ru Chen, Yue-Ting Chen, Yi-Chang Chen, Yu-Hsin Chu, Chia-Chen Chien, Po-Chen Chien, Shao-Yun Lo, Zhong-Liang Wang, Min-Chen Tsou, Ssu-Yu Chen, Guang-Shen Chiu, Wen-Ling Chen, Yi-Hsuan Wu, Lily Hui-Ching Wang, Wen-Ching Wang, Shu-Yi Lin, Hsing-Jien Kung, Lu-Hai Wang, Hui-Chun Cheng, Kai-Ti Lin. Hydrogen sulfide coordinates glucose metabolism switch through destabilizing tetrameric pyruvate kinase M2. Nature Communications. 2024;15(1).

10. Borbenyi-Galambos Klaudia, Erdelyi Katalin, Ditroi Tamás, Juranyi Eszter Petra, Szanto Noémi, Szatmari Réka, Czikora Ágnes, Schmidt Edward Eric, Garai Dorottya, Cserepes Mihály, Liszkay Gabriella, Toth Erika, Tovari József, Nagy Péter. Realigned transsulfuration drives BRAF-V600E-targeted therapy resistance in melanoma. Cell Metab. 2025;37(5):1171–88 e9.

11. Katalin Erdélyi Tamás Ditrói, Henrik J. Johansson, Ágnes Czikora, Noémi Balog , Laxmi Silwal-Pandit, Tomoaki Ida, Judit Olasz , Dorottya Hajdú, Zoltán Mátrai, Orsolya Csuka, Koji Uchida, József Tóvári, Olav Engebraten, Takaaki Akaike , Anne-Lise Børresen Dale, Miklós Kásler, Janne Lehtiö, Péter Nagy. Reprogrammed transsulfuration promotes basal-like breast tumor progression via realigning cellular cysteine persulfidation. Proc Natl Acad Sci U S A. 2021;118(45).

12. Czikora Ágnes, Erdelyi Katalin, Ditroi Tamás, Szanto Noémi, Juranyi Eszter Petra, Szanyi Szilárd, Tovari József, Strausz Tamás, Nagy Péter. Cystathionine beta-synthase overexpression drives metastatic dissemination in pancreatic ductal adenocarcinoma via inducing epithelial-to-mesenchymal transformation of cancer cells. Redox Biol. 2022;57:102505.

13. Péter Nagy Éva Dóka, Andrea Domán, Bindu D. Paul, József Balla, Michael P. Murphy, Christine Winterbourn, Rafael Radi, Solomon H. Snyder, Louis J. Ignarro, Helmut Sies Multifaceted roles for persulfide species in redox chemical biology. Nature Chemical Biology. 2026.

14. Takaaki Akaike Masanobu Morita, Seiryo Ogata, Jun Yoshitake, Minkyung Jung, Hiroki Sekine, Hozumi Motohashi, Uladzimir Barayeu, Tetsuro Matsunaga. New aspects

of redox signaling mediated by supersulfides in health and disease. Free Radic Biol Med. 2024;222:539–51.

15. Giuseppe Cirino Csaba Szabo, Andreas Papapetropoulos. Physiological roles of hydrogen sulfide in mammalian cells, tissues, and organs. Physiol Rev. 2023;103(1):31–276.

16. Jon M. Fukuto Louis J. Ignarro, Peter Nagy, David A. Wink, Christopher G. Kevil, Martin Feelisch, Miriam M. Cortese-Krott, Christopher L. Bianco, Yoshito Kumagai, Adrian J. Hobbs, Joseph Lin, Tomoaki Ida, Takaaki Akaike. Biological hydropersulfides and related polysulfides - a new concept and perspective in redox biology. FEBS Lett. 2018;592(12):2140–52.

17. Uladzimir Barayeu Danny Schilling, Mohammad Eid, Thamara Nishida Xavier da Silva, Lisa Schlicker, Nikolina Mitreska, Christopher Zapp, Frauke Gräter, Aubry K. Miller, Reinhard Kappl, Almut Schulze, José Pedro Friedmann Angeli, Tobias P. Dick. Hydropersulfides inhibit lipid peroxidation and ferroptosis by scavenging radicals. Nature Chemical Biology. 2023;19(1):28–37.

18. Zijun Wu Vinayak S Khodade, Jean-Philippe R Chauvin, Deborah Rodriguez, John P Toscano, Derek A Pratt. Hydropersulfides Inhibit Lipid Peroxidation and Protect Cells from Ferroptosis. J Am Chem Soc. 2022;144(34):15825–37.

19. Dan Wu Qingxun Hu, Deqiu Zhu An Update on Hydrogen Sulfide and Nitric Oxide Interactions in the Cardiovascular System. Oxidative Medicine and Cellular Longevity. 2018;2018.

20. Xue Guo Philip Schmiege, Tufa E Assafa, Rong Wang, Yan Xu, Linda Donnelly, Michael Fine, Xiaodan Ni, Jiansen Jiang, Glenn Millhauser, Liang Feng, Xiaochun Li. Structure and mechanism of human cystine exporter cystinosin. Cell. 2022;185(20):3739–52 e18.

21. Jan Lewerenz Sandra J Hewett, Ying Huang, Maria Lambros, Peter W Gout, Peter W Kalivas, Ann Massie, Ilse Smolders, Axel Methner, Mathias Pergande, Sylvia B Smith, Vadivel Ganapathy, Pamela Maher The cystine/glutamate antiporter system x(c)(-) in health and disease: from molecular mechanisms to novel therapeutic opportunities. Antioxid Redox Signal. 2013;18(5):522–55.

22. Pablo Martí-Andrés Isabela Finamor, Isabel Torres-Cuevas, Salvador Pérez, Sergio Rius-Pérez, Hildegard Colino-Lage, David Guerrero-Gómez, Esperanza Morato,

Anabel Marina, Patrycja Michalska , Rafael León, Qing Cheng , Eszter Petra Jurányi, Klaudia Borbényi-Galambos, Iván Millán, Péter Nagy, Antonio Miranda-Vizuete, Edward E Schmidt , Antonio Martínez-Ruiz , Elias Sj Arnér, Juan Sastre. TRP14 is the rate-limiting enzyme for intracellular cystine reduction and regulates proteome cysteinylation. EMBO J. 2024;43(13):2789–812.

23. Juan I Sbodio Solomon H Snyderó, Bindu D Paul. Regulators of the transsulfuration pathway. Br J Pharmacol. 2019;176(4):583–93.

24. Borbenyi-Galambos Klaudia, Czikora Ágnes, Erdelyi Katalin, Péter Nagy. Versatile roles of cysteine persulfides in tumor biology. Curr Opin Chem Biol. 2024;79:102440.

25. Pramod K Yadav Michael Martinov, Victor Vitvitsky, Javier Seravalli, Rudolf Wedmann, Milos R Filipovic, Ruma Banerjee. Biosynthesis and Reactivity of Cysteine Persulfides in Signaling. J Am Chem Soc. 2016;138(1):289–99.

26. Omer Kabil Ruma Banerjee. Enzymology of H2S biogenesis, decay and signaling. Antioxid Redox Signal. 2014;20(5):770–82.

27. Tomoaki Ida Tomohiro Sawa, Hideshi Ihara, Yukihiro Tsuchiya, Yasuo Watanabe, Yoshito Kumagai, Makoto Suematsu, Hozumi Motohashi, Shigemoto Fujii, Tetsuro Matsunaga, Masayuki Yamamoto, Katsuhiko Ono, Nelmi O. Devarie-Baez, Ming Xian, Jon M. Fukuto, and Takaaki Akaike. Reactive cysteine persulfides and S-polythiolation regulate oxidative stress and redox signaling. Proc Natl Acad Sci U S A. 2014;111(21):7606–11.

28. Takaaki Akaike Tomoaki Ida, Fan-Yan Wei, Motohiro Nishida, Yoshito Kumagai, Md. Morshedul Alam, Hideshi Ihara, Tomohiro Sawa, Tetsuro Matsunaga, Shingo Kasamatsu, Akiyuki Nishimura, Masanobu Morita, Kazuhito Tomizawa, Akira Nishimura, Satoshi Watanabe, Kenji Inaba, Hiroshi Shima, Nobuhiro Tanuma, Minkyung Jung, Shigemoto Fujii, Yasuo Watanabe, Masaki Ohmuraya, Péter Nagy, Martin Feelisch, Jon M. Fukuto, Hozumi Motohashi. Cysteinyl-tRNA synthetase governs cysteine polysulfidation and mitochondrial bioenergetics. Nat Commun. 2017;8(1):1177.

29. Kaylin G Fosnacht Jyoti Sharma, Pier Alexandre Champagne, Michael D Pluth. Transpersulfidation or H(2)S Release? Understanding the Landscape of Persulfide Chemical Biology. J Am Chem Soc. 2024;146(27):18689–98.

30. Ernesto Cuevasanta Matías N Möller, Beatriz Alvarez. Biological chemistry of hydrogen sulfide and persulfides. Biochemistry and Biophysics. 2017;617:9–25.
31. Zhichao Liu Nicolas Rouhier, Jérémy Couturier. Dual Roles of Reducing Systems in Protein Persulfidation and Depersulfidation. Antioxidants (Basel). 2025;14(1).
32. Éva Dóka Irina Pader, Adrienn Bíró, Katarina Johansson, Qing Cheng, Krisztina Ballagó, Justin R Prigge, Daniel Pastor-Flores, Tobias P Dick, Edward E Schmidt, Elias S J Arnér, Péter Nagy. A novel persulfide detection method reveals protein persulfide- and polysulfide-reducing functions of thioredoxin and glutathione systems. Sci Adv. 2016;2(1):e1500968.
33. Jumi Lee Inhwan Yoo, Ihyeon Ahn, Namgyu Lee. Promiscuous enzyme SQOR in cellular metabolism and ferroptosis regulation. BMB Rep. 2025;58(6):233–7.
34. Marouane Libiad Victor Vitvitsky, Trever Bostelaar, Daniel W Bak, Ho-Joon Lee, Naoya Sakamoto, Eric Fearon, Costas A Lyssiotis, Eranthie Weerapana, Ruma Banerjee. Hydrogen sulfide perturbs mitochondrial bioenergetics and triggers metabolic reprogramming in colon cells. J Biol Chem. 2019;294(32):12077–90.
35. Joseph V Roman Yashvi Shukla, David A Hanna, Mackenzie Mackson, Tsz-Leung To, Vamsi Mootha, Ruma Banerjee. Hydrogen sulfide-dependent activation of human sulfide quinone oxidoreductase. J Biol Chem. 2025;301(10):110681.
36. Dayana Benchoam Ernesto Cuevasanta, Joseph V Roman, Ruma Banerjee, Beatriz Alvarez. Acidity of persulfides and its modulation by the protein environments in sulfide quinone oxidoreductase and thiosulfate sulfurtransferase. J Biol Chem. 2024;300(5):107149.
37. Doka Éva, Ida Tomohiro, Dagnell Magnus, Abiko Yasuhiro, Luong Ngo Cao, Balog Noémi, Takata Takashi, Espinosa Bárbara, Nishimura Akira, Cheng Qing, Funato Yasuhiro , Miki Hiroaki , Fukuto Jon M., Prigge Justin R., Schmidt Edward Eric, Arner Elias. S. J., Kumagai Y., Akaike Takaaki, Nagy Péter. Control of protein function through oxidation and reduction of persulfidated states. Sci Adv. 2020;6(1):eaax8358.
38. Navasona Krishnan Cexiong Fu, Darryl J Pappin, Nicholas K Tonks. H2S-Induced Sulfhydration of the Phosphatase PTP1B and Its Role in the Endoplasmic Reticulum Stress Response. Science Signaling. 2011;4(203).
39. Tomohiro Sawa Tsuyoshi Takata, Tetsuro Matsunaga, Hideshi Ihara, Hozumi Motohashi, Takaaki Akaike Chemical Biology of Reactive Sulfur Species: Hydrolysis-

Driven Equilibrium of Polysulfides as a Determinant of Physiological Functions. Antioxid Redox Signal. 2022;36(4-6):327–36.

40. Vignane Thibaut, Filipovic Milos R. Emerging Chemical Biology of Protein Persulfidation. Antioxid Redox Signal. 2023;39(1-3):19–39.

41. Anita Vasas, Éva Dóka István Fábián, Péter Nagy. Kinetic and thermodynamic studies on the disulfide-bond reducing potential of hydrogen sulfide. Nitric Oxide. 2015;46:93–101.

42. Asif K Mustafa Moataz M Gadalla, Nilkantha Sen, Seyun Kim, Weitong Mu, Sadia K Gazi, Roxanne K Barrow, Guangdong Yang, Rui Wang, Solomon H Snyder. H2S signals through protein S-sulfhydration. Sci Signal. 2009;2(96):ra72.

43. Brandán Pedre Deepti Talwar, Uladzimir Barayeu, Danny Schilling, Marcin Luzarowski, Mikolaj Sokolowski, Sebastian Glatt, Tobias P. Dick. 3-Mercaptopyruvate sulfur transferase is a protein persulfidase. Nature Chemical Biology. 2023;19(4):507–17.

44. Yuka Kimura Shin Koike, Norihiro Shibuya, David Lefer, Yuki Ogasawara, Hideo Kimura. 3-Mercaptopyruvate sulfurtransferase produces potential redox regulators cysteine- and glutathione-persulfide (Cys-SSH and GSSH) together with signaling molecules H(2)S(2), H(2)S(3) and H(2)S. Sci Rep. 2017;7(1):10459.

45. Jasmina Zivanovic Emilia Kouroussis, Joshua B Kohl, Bikash Adhikari, Biljana Bursac, Sonia Schott-Roux, Dunja Petrovic, Jan Lj Miljkovic, Daniel Thomas-Lopez, Youngeun Jung, Marko Miler, Sarah Mitchell, Verica Milosevic, Jose Eduardo Gomes, Moran Benhar, Bruno Gonzalez-Zorn, Ivana Ivanovic-Burmazovic, Roberta Torregrossa, James R Mitchell, Matthew Whiteman, Guenter Schwarz, Solomon H Snyder, Bindu D Paul, Kate S Carroll, Milos R Filipovic Selective Persulfide Detection Reveals Evolutionarily Conserved Antiaging Effects of S-Sulfhydration. Cell Metab. 2019;30(6):1152–70 e13.

46. Nagy Péter, Schwarz Günter, Kopriva Stanislav. Highlighted mechanistic aspects in the chemical biology of reactive sulfur species. Br J Pharmacol. 2019;176(4):511–3.

47. Yasuhiro Shinkai Yoshito Kumagai. Sulfane Sulfur in Toxicology: A Novel Defense System Against Electrophilic Stress. Toxicol Sci. 2019;170(1):3–9.

48. Jon M Fukuto Adrian J Hobbs. A comparison of the chemical biology of hydropersulfides (RSSH) with other protective biological antioxidants and nucleophiles. Nitric Oxide. 2021;107:46–57.

49. Dayana Benchoam Jonathan A Semelak, Ernesto Cuevasanta, Mauricio Mastrogiovanni, Juan S Grassano, Gerardo Ferrer-Sueta, Ari Zeida, Madia Trujillo, Matías N Möller, Darío A Estrin, Beatriz Alvarez. Acidity and nucleophilic reactivity of glutathione persulfide. J Biol Chem. 2020;295(46):15466–81.

50. Ernesto Cuevasanta Mike Lange, Jenner Bonanata, E Laura Coitiño, Gerardo Ferrer-Sueta, Milos R Filipovic, Beatriz Alvarez. Reaction of Hydrogen Sulfide with Disulfide and Sulfenic Acid to Form the Strongly Nucleophilic Persulfide. J Biol Chem. 2015;290(45):26866–80.

51. Chauvin Jean-Philippe R., Griesser Markus, Pratt Derek. A. The antioxidant activity of polysulfides: it's radical! Chem Sci. 2019;10(19):4999–5010.

52. Christopher L. Bianco, Tyler A. Chavez Victor Sosa, Simran, S. Saund , Q. Nhu N. Nguyen, Dean J. Tantillo, , Andrew S. Ichimura John P. Toscano, Jon M. Fukuto. The chemical biology of the persulfide (RSSH)/perthiyl (RSS.) redox couple and possible role in biological redox signaling. Free Radic Biol Med. 2016;101:20–31.

53. Wu Zijun, Pratt Derek A. Radical Substitution Provides a Unique Route to Disulfides. J Am Chem Soc. 2020;142(23):10284–90.

54. Nagy Péter. Kinetics and mechanisms of thiol-disulfide exchange covering direct substitution and thiol oxidation-mediated pathways. Antioxid Redox Signal. 2013;18(13):1623–41.

55. Dayana Benchoam Ernesto Cuevasanta, Matías N Möller, Beatriz Alvarez. Persulfides, at the crossroads between hydrogen sulfide and thiols. Essays Biochem. 2020;64(1):155–68.

56. Chun-Yu Fu Joshua B Kohl, Filip Liebsch, Davide D'Andrea, Tamás Ditrói, Seiryo Ogata, Franziska Neuser, Max Mai, Anna T Mellis, Emilia Kouroussis, Masanobu Morita, Titus Gehling, José Angel Santamaria-Araujo, Sin Yuin Yeo, Heike Endepols, Michaela Křížková, Viktor Kozich, Marcus Krueger, Julia B Hennermann, Uladzimir Barayeu, Takaaki Akaike, Peter Nagy, Milos Filipovic, Guenter Schwarz Sulfite oxidase deficiency causes persulfidation loss and hydrogen sulfide release. Journal of Clinical Investigation. 2025;135(21).

57. Virág Bogdándi Tomoaki Ida, Thomas R Sutton, Christopher Bianco, Tamás Ditrói, Grielof Koster, Hillary A Henthorn, Magda Minnion, John P Toscano, Albert van der Vliet, Michael D Pluth, Martin Feelisch, Jon M Fukuto, Takaaki Akaike, Péter Nagy. Speciation of reactive sulfur species and their reactions with alkylating agents: do we have any clue about what is present inside the cell? Br J Pharmacol. 2019;176(4):646–70.

58. Danny Schilling Uladzimir Barayeu, Raphael R Steimbach, Deepti Talwar, Aubry K Miller, Tobias P Dick. Commonly Used Alkylating Agents Limit Persulfide Detection by Converting Protein Persulfides into Thioethers. Angewandte Chemie-International Edition. 2022;61(30).

59. Schilling Danny, Ditroi Tamás, Barayeu Uladzimir, Juranyi Eszter Petra, Nagy Péter, Dick Tobias P. The influence of alkylating agents on sulfur-sulfur bonds in per- and polysulfides. Curr Opin Chem Biol. 2023;76:102368.

60. Ryosuke Kawagoe Ippei Takashima, Shohei Uchinomiyaa, Akio Ojida. Reversible ratiometric detection of highly reactive hydropersulfides using a FRET-based dual emission fluorescent probe. Chem Sci. 2017;8(2):1134–40.

61. Raevskii Roman I., Katrukha Veronika, Khramova Yulia, Bilan Dmitry. Biochemistry of Redox-Active Sulfur Compounds in Mammalian Cells and Approaches to Their Detection (A Review). Russian Journal of Bioorganic Chemistry. 2024;50(4):1237–62.

62. Meg Shieh, Xiang Ni, Shi Xu, Stephen P. Lindahl, Moua Yang, Tetsuro Matsunaga Robert Flaumenhaft, Takaaki Akaike, Ming Xian. Shining a light on SSP4: A comprehensive analysis and biological applications for the detection of sulfane sulfurs. Redox Biol. 2022;56:102433.

63. Nagy Péter, Dóka Éva, Ida Tomohiro, Akaike Takaaki. Measuring Reactive Sulfur Species and Thiol Oxidation States: Challenges and Cautions in Relation to Alkylation-Based Protocols. Antioxidants & Redox Signaling. 2020;33(16):1174–89.

64. Aggarwal Sahil C., Khodade Vinayak S., Porche Sarah., Pharoah Blaze M., Toscano John P. Photochemical Release of Hydropersulfides. J Org Chem. 2022;87(19):12644–52.

65. Ling Fu Keke Liu, Jingyang He, Caiping Tian, Xiaobo Yu, Jing Yang Direct Proteomic Mapping of Cysteine Persulfidation. Antioxid Redox Signal. 2020;33(15):1061–76.

66. Sofia Iris Bibli Jiong Hu, Mario Looso, Andreas Weigert, Corina Ratiu, Janina Wittig, Maria Kyriaki Drekolia, Lukas Tombor, Voahanginirina Randriamboavonjy, Matthias S. Leisegang, Philipp Goymann, Fredy Delgado Lagos, Beate Fisslthaler, Sven Zukunft, Anastasia Kyselova, Alberto Fernando Oliveira Justo, Juliana Heidler, Diamantis Tsilimigras, Ralf P. Brandes, Stefanie Dimmeler Andreas Papapetropoulos, Stefan Knapp, Stefan Offermanns, Ilka Wittig, Stephen L. Nishimura, Fragiska Sigala, Ingrid Fleming. Mapping the Endothelial Cell-Sulfhydrome Highlights the Crucial Role of Integrin Sulfhydration in Vascular Function. Circulation. 2021;143(9):935–48.

67. Rudolf Wedmann Constantin Onderka, Shengwei Wei, István András Szijártó, Jan Lj. Miljkovic, Aleksandra Mitrovic, Mike Lange, Sergey Savitsky, Pramod Kumar Yadav, Roberta Torregrossa, Ellen G. Harrer, Thomas Harrer, Isao Ishii, Maik Gollasch, Mark E. Wood, Erwan Galardon, Ming Xian, Matthew Whiteman, Ruma Banerjeed , Milos R. Filipovic. Improved tag-switch method reveals that thioredoxin acts as depersulfidase and controls the intracellular levels of protein persulfidation. Chem Sci. 2016;7(5):3414–26.

68. Dehui Zhang Igor Macinkovic, Nelmi O Devarie-Baez, Jia Pan, Chung-Min Park, Kate S Carroll, Milos R Filipovic, Ming Xian. Detection of protein S-sulfhydration by a tag-switch technique. Angew Chem Int Ed Engl. 2014;53(2):575–81.

69. Tsuyoshi Takata, Minkyung Jung, Tetsuro Matsunaga Tomoaki Ida, Masanobu Morita, Hozumi Motohashi, Xinggui Shen Christopher G. Kevil, Jon M. Fukuto, Takaaki Akaike Methods in sulfide and persulfide research. Nitric Oxide. 2021;116:47–64.

70. Shingo Kasamatsu Tomoaki Ida, Taisei Koga, Kosho Asada, Hozumi Motohashi, Hideshi Ihara, and Takaaki Akaike. High-Precision Sulfur Metabolomics Innovated by a New Specific Probe for Trapping Reactive Sulfur Species. Antioxid Redox Signal. 2021;34(18):1407–19.

71. Jan Lj. Miljkovic Nils Burger, Chak Shun Yu, Alexander H. Harkiss, Stefan Warrington, Stuart T. Caldwell, Scott A. Jones, Jordan J. Lee, Dunja Aksentijevic, Andrew M. James, Thomas Krieg, Richard C. Hartley, Michael P. Murphy. Simultaneous

and sensitive quantification of protein and low molecular weight persulfides, polysulfides and H(2)S in biological samples. Nat Commun. 2025;17(1):85.

72. Hisyam Abdul Hamid, Akira Tanaka Tomoaki Ida, Akira Nishimura, Tetsuro Matsunaga Shigemoto Fujii, Masanobu Morita, Tomohiro Sawa, Jon M. Fukuto, Péter Nagy, , Ryouhei Tsutsumi Hozumi Motohashi, Hideshi Ihara, Takaaki Akaike Polysulfide stabilization by tyrosine and hydroxyphenyl-containing derivatives that is important for a reactive sulfur metabolomics analysis. Redox Biol. 2019;21:101096.

73. Sofi Eriksson Justin R. Prigge, Emily A. Talago, Elias S.J. Arnér, Edward E. Schmidt. Dietary methionine can sustain cytosolic redox homeostasis in the mouse liver. Nat Commun. 2015;6:6479.

74. Edward E. Schmidt Eszter Petra Jurányi, Colin G. Miller, Sydney A. Austad, Tamás Ditrói, Zoe M. Seaford, Sang Jun Yoon, Reed C. Noyd, Yun Pyo Kang, Justin R. Prigge, Vivien Csikós, Martina Serrano Alvarez, Katalin Erdélyi, Dóra Kővári, Gina M. DeNicola, Peter Nagy. Cystine C-S bond cleavage fuels cysteine production under disulfide reductase deficiency. Nature Chemical Biology. 2026.

75. Mingxiao Feng Sara Divall, Sheng Wu. An Improved Time- and Labor- Efficient Protocol for Mouse Primary Hepatocyte Isolation. J Vis Exp. 2021(176).

76. Shafiul Alam Sibile Pardue, Xinggui Shen, John D Glawe, Takashi Yagi, Mohammad Alfrad Nobel Bhuiyan, Rakesh P Patel, Paari S Dominic, Chiranjiv S Virk, Md Shenuarin Bhuiyan, A Wayne Orr, Chad Petit, Gopi K Kolluru, Christopher G Kevil. Hypoxia increases persulfide and polysulfide formation by AMP kinase dependent cystathionine gamma lyase phosphorylation. Redox Biol. 2023;68:102949.

77. Tamás Ditrói Attila Nagy, Diego Martinelli, András Rosta, Viktor Kožich, Péter Nagy. Comprehensive analysis of how experimental parameters affect H(2)S measurements by the monobromobimane method. Free Radic Biol Med. 2019;136:146–58.

78. Joseph Lin Masahiro Akiyama, Iris Bica, Faith T Long, Catherine F Henderson, Robert N Goddu, Valeria Suarez, Blaine Bake, Tomoaki Ida, Yasuhiro Shinkai, Peter Nagy, Takaaki Akaike, Jon M Fukuto, Yoshito Kumagai. The Uptake and Release of Polysulfur Cysteine Species by Cells: Physiological and Toxicological Implications. Chem Res Toxicol. 2019;32(3):447–55.

79. Torsten Müller Dominic Winter. Systematic Evaluation of Protein Reduction and Alkylation Reveals Massive Unspecific Side Effects by Iodine-containing Reagents. Mol Cell Proteomics. 2017;16(7):1173–87.

9 Bibliography of the candidate's publications

9.1 Publications related to the thesis

Schmidt Edward E, Jurányi Eszter Petra, Miller Colin G, Austad Sydney A, Ditrói Tamás, Seaford Zoe M, Yoon Sang Jun, Noyd Reed C, Kang Yun Pyo, Prigge Justin R, Csikós Vivien, Serrano Alvarez Martina, Erdélyi Katalin, Kővári Dóra, DeNicola Gina M, Nagy Peter

Cystine C-S bond cleavage fuels cysteine production under disulfide reductase deficiency

NATURE CHEMICAL BIOLOGY (1552-4450 1552-4469): (2026) IF: 13.7

Czikora Ágnes, Erdélyi Katalin, Ditrói Tamás, Szántó Noémi, Jurányi Eszter Petra, Szanyi Szilárd, Tóvári József, Strausz Tamás, Nagy Péter

Cystathionine β-synthase overexpression drives metastatic dissemination in pancreatic ductal adenocarcinoma via inducing epithelial-to-mesenchymal transformation of cancer cells.

REDOX BIOLOGY 57 Paper: 102505, 14 p. (2022) IF: 11.4

9.2 Publications not related to the thesis

Borbényi-Galambos Klaudia, Erdélyi Katalin, Ditrói Tamás, Jurányi Eszter Petra, Szántó Noémi, Szatmári Réka, Czikora Ágnes, Schmidt Edward E., Garai Dorottya, Cserepes Mihály, Liszkay Gabriella, Tóth Erika, Tóvári József, Nagy Péter
Realigned transsulfuration drives BRAF-V600E-targeted therapy resistance in melanoma
CELL METABOLISM 37: 5 pp. 1177-1188.e9. , 12 p. (2025) IF: 30.9

Martí-Andrés Pablo, Finamor Isabela, Torres-Cuevas Isabel, Pérez Salvador, Rius-Pérez Sergio, Colino-Lage Hildegard, Guerrero-Gómez David, Morato Esperanza, Marina Anabel, Michalska Patrycja, León Rafael, Cheng Qing, Jurányi Eszter Petra, Borbényi-Galambos Klaudia, Millán Iván, Nagy Péter, Miranda-Vizuete Antonio, Schmidt Edward E, Martínez-Ruiz Antonio, Arnér Elias Sj, Sastre Juan

TRP14 is the rate-limiting enzyme for intracellular cystine reduction and regulates proteome cysteinylation.

EMBO JOURNAL 43: 13 pp. 2789-2812. , 24 p. (2024) IF: 8.3

Panagaki Theodora, Janickova Lucia, Petrovic Dunja, Zuhra Karim, Ditrói Tamás, Jurányi Eszter Petra, Bremer Olivier, Ascenção Kelly, Philipp Thilo M, Nagy Péter, Filipovic Milos R, Szabo Csaba

Neurobehavioral dysfunction in a mouse model of Down syndrome: upregulation of cystathionine β-synthase, H_2S overproduction, altered protein persulfidation, synaptic dysfunction, endoplasmic reticulum stress, and autophagy

GEROSCIENCE: OFFICIAL JOURNAL OF THE AMERICAN AGING ASSOCIATION (AGE) 46: 5 pp. 4275-4314. , 40 p. (2024) IF: 5.4

Combi Zsolt, Potor László, Nagy Péter, Sikura Katalin Éva, Ditrói Tamás, Jurányi Eszter Petra, Galambos Klaudia, Szerafin Tamás, Gergely Péter, Whiteman Matthew, Torregrossa Roberta, Ding Yuchao, Beke Lívia, Hendrik Zoltán, Méhes Gábor, Balla György, Balla József

Hydrogen sulfide as an anti-calcification stratagem in human aortic valve: Altered biogenesis and mitochondrial metabolism of H_2S lead to H_2S deficiency in calcific aortic valve disease

REDOX BIOLOGY 60 Paper: 102629, 19 p. (2023) IF: 10.7

Orján Erik Márk, Kormányos Eszter Sára, Fűr Gabriella Mihalekné, Dombi Ágnes, Bálint Emese Réka, Balla Zsolt, Balog Beáta Adél, Dágó Ágnes, Totonji Ahmad, Bátai Zoárd István, Jurányi Eszter Petra, Ditrói Tamás, Al-Omari Ammar, Pozsgai Gábor, Kormos Viktória, Nagy Péter, Pintér Erika, Rakonczay Zoltán, Kiss Lóránd

The anti-inflammatory effect of dimethyl trisulfide in experimental acute pancreatitis

SCIENTIFIC REPORTS 13: 1 Paper: 16813, 19 p. (2023) IF: 3.8

Schilling Danny, Ditrói Tamás, Barayeu Uladzimir, Jurányi Eszter Petra, Nagy Peter, Dick Tobias P

The influence of alkylating agents on sulfur-sulfur bonds in per- and polysulfides

CURRENT OPINION IN CHEMICAL BIOLOGY 76 Paper: 102368, 8 p. (2023) IF: 6.9

10 Acknowledgements

I am grateful to my supervisor, Professor Péter Nagy, for his continuous guidance, support, and encouragement throughout my PhD journey. I truly appreciate the trust he invested in me and the valuable professional knowledge he shared, which greatly enriched my scientific thinking and understanding of research. I am especially grateful for the freedom to explore and test my own ideas.

I would like to thank Tamás Ditrói, from whom I learned many skills, including technical expertise, HPLC-MS/MS operation, experimental design, and data analysis.

I truly appreciate Klaudia Borbényi-Galambos and Noémi Szántó for generously providing cells for my experiment and for always being there to help me manage all my samples.

I would like to express my gratitude to Professor Edward Schmidt for his invaluable contributions to this work. He developed the mouse models, and his dedication to conducting most of the animal experiments was essential to the success of this project. I also appreciate our brainstorming sessions.

To the MITO, I'm truly thankful for the supportive, cheerful, and inspiring environment you've created. Thank you for your ongoing support of both my work and my well-being, Noémi Szántó, Klaudia Borbényi-Galambos, Réka Zsuzsanna Szatmári, Zsuzsanna Lénárt, Tamás Ditrói, Laura Somodi, Annamária Hakl, Ágnes Czikora, Katalin Erdélyi, Dorottya Garai, Éva Ditróiné Dóka, Andrea Domán, Zsuzsanna Gyöngy, Daniella Dörgő, and Kevin Dósa.

Last, but not least, I want to warmly thank my family for their constant support during my PhD journey, I truly appreciate their patience in not asking, "When will you complete your PhD?" so often. I am very grateful to my friends, especially Áron and Peti, for their constant motivation and presence, which kept me going through the most challenging times of my doctoral studies.